The Anti-Dysenteric Drug Fraxetin Enhances Anti-Tumor Efficacy of Gemcitabine and Suppresses Pancreatic Cancer Development by Antagonizing STAT3 Activation

Yangyang Guo
Wenzhou Medical University First Affiliated Hospital: The First Affiliated Hospital of Wenzhou Medical University
Yanyi Xiao
Wenzhou Medical University First Affiliated Hospital: The First Affiliated Hospital of Wenzhou Medical University
Hangcheng Guo
Wenzhou Medical University First Affiliated Hospital: The First Affiliated Hospital of Wenzhou Medical University
Hengyue Zhu
Wenzhou Medical University First Affiliated Hospital: The First Affiliated Hospital of Wenzhou Medical University
Dong Chen
The Sixth People's Hospital of Wenzhou City
Jilong Wang
University of Chinese Academic Science
Junjie Deng
University of Chinese Academic Science
Zheng Xu
Wenzhou Medical University First Affiliated Hospital: The First Affiliated Hospital of Wenzhou Medical University
Junjie Lan
Xiamen University
Xiaodong Liu
Wenzhou Medical University
Qiyu Zhang
Wenzhou Medical University First Affiliated Hospital: The First Affiliated Hospital of Wenzhou Medical University
Yongheng Bai (wzbyh@wmu.edu.cn)
The First Affiliated Hospital of Wenzhou Medical University

Research

Keywords: Fraxetin, Pancreatic ductal adenocarcinoma, Gemcitabine, STAT3, Oxidative stress

Posted Date: December 15th, 2020

DOI: https://doi.org/10.21203/rs.3.rs-125318/v1

Abstract

Background

Fraxetin, a natural product isolated and purified from the bark of *Fraxinus bungeana A.DC.*, has anti-inflammatory, analgesic and anti-dysenteric activities. This study aimed to investigate the anti-tumor effects of fraxetin in pancreatic ductal adenocarcinoma (PDA) and elucidate the underlying molecular mechanism.

Methods

The effects of quercetin on the proliferation, apoptosis, migration and invasion of pancreatic cancer cells (PCCs), and tumor growth and metastasis in PDA xenograft mouse models were evaluated. Besides, the effects of fraxetin on the sensitivity of PCCs to gemcitabine were evaluated. Moreover, angiogenesis, glucose metabolism, the epithelial-mesenchymal transition (EMT), reactive oxygen species (ROS), and STAT3 activity were analyzed.

Results

In PCCs, fraxetin inhibited the proliferation, induced mitochondrial-dependent apoptosis, and suppressed the invasion and migration by reversing the EMT. In nude mouse models, PDA growth and metastasis were reduced by fraxetin treatment. Moreover, fraxetin enhanced the sensitivity of PCCs to the chemotherapy drug gemcitabine. Mechanically, oncogenic KRAS-triggered STAT3 activation in PCCs and PDA tissues was suppressed by fraxetin treatment. Fraxetin shows important interactions with STAT3 Src Homology 2 (SH2) domain residues to occupy the pTyr-recognition site of its SH2 domain of another STAT3 monomer, thereby preventing its homo-dimer formation, which then blocks the activation of downstream signal pathways. The anti-tumor activity of fraxetin in PDA was functionally rescued by a STAT3 activator colivelin. As a result, fraxetin hindered hypoxia-induced angiogenesis by decreasing HIF-1α and VEGFA expression, controlled glucose metabolism by reducing GLUT1 expression, inhibited the EMT by blocking the Slug-E-cadherin axis, and drove ROS-mediated apoptosis by regulating STAT3-Ref1 axis.

Conclusion

These findings indicate that fraxetin enhances anti-tumor activity of gemcitabine and suppresses pancreatic cancer development by antagonizing STAT3 activation.

Background

Pancreatic ductal adenocarcinoma (PDA) is a highly-malignant tumor of the digestive system with a very poor prognosis and high mortality [1]. However, the underlying mechanism of PDA development remains unclear [2]. Surgery clinically is regarded as the main treatment for PDA. However, only a few PDA patients can receive surgery. Patients who are unable to undergo surgery presently receive a combination

of radiation and chemotherapy drugs, such as gemcitabine [3]. These adjuvant treatments can inhibit, to some extent, the further deterioration of PDA patients, but whether they can prolong the life of patients requires further clinical observations [4]. Therefore, it is urgent to develop new treatments and effective drugs for PDA.

The Janus kinase-2 (JAK2)/signal transducer and activator of transcription-3 (STAT3) signaling pathway takes part in diverse physiological processes, such as cellular proliferation, differentiation, apoptosis, and migration in mammals [5]. In response to a variety of cytokines or related factors (e.g., interferon, interleukins), JAK2 protein is activated via phosphorylation at two adjacent tyrosine residues, and then phosphorylates and activates cytoplasmic STAT3 protein. Activated STAT3 can transfer into the nucleus to bind specific regulatory sequences to activate or suppress transcription of target genes, such as c-Myc and cyclin D1 [6–9]. As a result, activated STAT3 plays a crucial role in the regulation of the cell cycle, apoptosis and angiogenesis [10]. A series of studies have shown that in human PDA tissues the STAT3 is overactivated [11, 12], which may be caused by oncogenic KRAS mutation [13]. STAT3 controls several downstream oncogenic signaling pathways and is required for triggering pancreatic intraepithelial neoplasia progression to an invasive PDA [13]. Thus, targeting STAT3 may be an effective strategy for the treatment of PDA progression.

Fraxetin is a plant-derived coumarin primarily isolated from *Fraxinus bungeana A.DC.*, and has been reported to exert potential anti-bacterial, neuroprotective, anti-inflammatory, and anti-dysenteric activities [14]. Recently, several studies have demonstrated that fraxetin suppresses tumor growth and metastasis in multiple cancer types [15, 16]. Importantly, STAT3 was involved in fraxetin-mediated inhibitory effects on the proliferation of non-small-cell lung cancer cells [17]. Considering aberrant activation of STAT3 in PDA, we hypothesized that fraxetin might have the potential to protect against PDA progression by suppressing STAT3 activity.

In this study, we aimed to investigate the effects of fraxetin on PDA *in vitro* and *in vivo* and further elucidated the underlying molecular mechanism. Besides, the effects of fraxetin on the sensitivity of PCCs to the chemotherapy drug gemcitabine were evaluated. Moreover, angiogenesis, glucose metabolism, the epithelial-mesenchymal transition (EMT), reactive oxygen species (ROS), and STAT3 activity were analyzed. Our results revealed that fraxetin enhanced the anti-tumor efficacy of gemcitabine and suppressed oncogenesis and development of PDA by antagonizing STAT3 activation.

Materials And Methods

Cells culture and drug treatment

Human PCC lines PANC-1 and Patu8988, which have strong proliferative and invasive abilities [18], were obtained from the Cell Bank of the Chinese Academy of Sciences (Shanghai, China). Cells were routinely cultured in Dulbecco's Modified Eagle Medium (DMEM, Invitrogen, Carlsbad, CA, USA) supplemented with 10% fetal bovine serum (FBS, Invitrogen), 100 U ml^{-1} penicillin and 100 μg ml^{-1} streptomycin

(Invitrogen). PANC-1 and Patu8988 cells were plated at a density of 1×10^6 and preincubated for 24 h at 37 °C, in the complete medium containing 5% FBS at approximately 70% confluence in culture plates. After 24 h, the complete medium was replaced with serum-free medium for 24 h before drug treatment. PANC-1 and Patu8988 cells were treated with 50 or 100 μM fraxetin (Fig. 1A, CAS#: 574-84-5, Purity: ≥98% by HPLC, Yuanye Biotechnology, Shanghai, China) with or without colivelin (CAS#: 867021-83-8, MedChemExpress, NJ, USA).

Cell Counting Kit-8 assay

To measure the viability of PANC-1 and Patu8988 cells, the Cell Counting Kit-8 (CCK-8) for cell proliferation and cytotoxicity assay kit (Dojindo, Shanghai, Japan) was performed as per the manufacturer's instructions. Firstly, cells were plated in DMEM medium for 24 h followed by incubation in 96-well plates. Secondly, incubated cells were added to the plates at a density of 5×10^3 cells/well and then were treated with different concentrations of fraxetin for 24 h. At appropriate time points, 10 μl of this reagent was added per well and incubated for another 2 h. Finally, the absorbance at 450 nm was determined. The cell viability was calculated by comparing the experimental cells with untreated control cells. All experiments were repeated at least in triplicate.

Cell apoptosis analysis

PANC-1 and Patu8988 cells were cultured in DMEM with different concentrations of fraxetin for 24 h, and then were collected by centrifugation. For apoptosis analysis, Annexin V-FITC (Multi Science, Hangzhou, China) was added to resuspended cells at room temperature, and incubated for 15 min in the dark. Next, propidium iodide (PI, Multi Science) was added to resuspended cells, and incubated for another 5 min in the dark. Finally, cell apoptosis was analyzed using flow cytometry (Ex = 488 nm; Em = 530 nm, BD FACSVerse™, BD Biosciences, San Jose, CA, USA).

Real-time cellular analysis

PANC-1 or Patu8988 cells were seeded at a density of 4×10^3 cells/well in cell culture E16-Plate (ACEA Biosciences, San Diego, CA, USA), and then cellular growth index was recorded by Label-free Real-time Cellular Analysis System (RTCA; Roche, Penzberg, Germany) automatically.

Transwell invasion assay

A transwell chamber (Costar, New York City, NY, USA) assay was performed in a 24-well plate. The transwell inserts were coated with 150 μl Matrigel at 37˚C for 2 h. PANC-1 and Patu8988 cells (4×10^5) were collected and resuspended in a serum-free medium supplemented with fraxetin. Cells were incubated in the upper chamber, and the lower chamber was infused with 500 μl DMEM containing 10% FBS. The transwell plate was incubated at 37˚C for 24 h, and then removed the gel and cells in the upper chamber. After formalin fixation, crystal violet (Sigma-Aldrich, USA) was used to stain the membrane for 10 min. Finally, the number of invaded cells in six randomly selected fields was counted using a microscope (Leica Microsystems, Wetzlar, Germany).

Colony formation assay

PANC-1 or Patu8988 cells were plated in 6-well plates at a density of 1×10^3 cells/well for 24 h, and then were treated with fraxetin. After treatment for 24 h, the culture medium was placed with DMEM for 14 days. Colonies were fixed with formaldehyde for 30 min and stained with crystal violet (Sigma-Aldrich). Finally, cell colonies were counted using a microscope (Leica Microsystems).

Wound healing assay

PANC-1 or Patu8988 cells were seeded in 6well plates and maintained at 37˚C for 24 h. The culture area was scratched using a crystal pipette tip to make a linear gap among the cells. Next, the detached cells washed away with PBS and then added different concentrations of fraxetin. Cells were allowed to fill the gap, and after 24 h, images of the culture area were captured using a microscope (Leica Microsystems).

Immunocytochemical staining

Immunofluorescence staining was performed according to our previous report [19]. Firstly, PANC-1 and Patu8988 cells treated with fraxetin were grown on glass coverslips for 24 h, and then fixed with 4% formaldehyde for 30 min. Secondly, cells were permeabilized with 0.1% Triton X-100, and blocked in 4% normal goat serum for 1.5 h. PANC-1 and Patu8988 cells were incubated overnight at 4 °C with primary antibodies against Ki67 (1:150, Abcam, Cambridge, MA, USA), Ref1 (1:200, Abcam), STAT3 (1:200, Cell Signaling Technology, CST, Beverly, MA, USA), E-cadherin (1:200, Abcam), and Vimentin (1:200, Abcam) followed by incubation at room temperature with secondary antibody (1:400) for 1 h. Finally, cells were stained with 4'6-diamidino-2-phenylindole (DAPI, Beyotime Biotechnology, Shanghai, China), and Ki67-positive cells were counted using a microscope (Leica Microsystems).

Glucose metabolism assay

The intact cellular oxygen consumption rate (OCR) and extracellular acidification rate (ECAR) were measured using a Seahorse XF96 Extracellular Flux Analyser (Seahorse Bioscience, North Billerica, MA, USA). In short, 1.0×10^4 of PANC-1 and Patu8988 cells were seeded into 96-well cell plates and incubated overnight at 37 ℃, 5% CO_2. Both cells were pretreated with or without different concentrations of fraxetin for 24 hours. Simultaneously, the calibration plates were incubated overnight at 37 ℃ in a non-CO_2 incubator. Then both cell mediums were replaced with assay medium, once the probe calibration was completed, the cell plate replaced the probe plate. The analyzer plotted the value of OCR followed by injection of the compounds sequentially as follows: oligomycin (inhibitor of ATP synthase; 2.5 μM), Carbonyl cyanide 4-(trifluoromethoxy) phenylhydrazone (FCCP, an uncoupler of OXPHOS; 2 μM), rotenone (inhibitor of complex I; 0.25 μM) and anti-mildew A (inhibitor of complex III; 0.25 μM) (n = 8). ECAR was evaluated after continuous injection of glucose (10 mM), oligomycin (1 μM) and 2-Deoxyglucose 2-Deoxyglucose (2-DG, 50 mM) (n = 8). After completing the test, the BCA Protein Assay Kit was performed to determine protein concentration to normalize OCR and ECAR according to the manufacturer's instructions.

Nude mouse tumorigenicity

Male nude mice (BALB/c) weighing 20–22 g and 6–8 weeks old were obtained from the Experimental Animal Centre of Wenzhou Medical University (Wenzhou, China). All mice were housed in a humidity-, temperature-, and light-controlled environment. Mice were randomly divided into two groups and each group contained five mice. Then the right thigh root of mice was injected subcutaneously with 3×10^6 PANC-1 cells. The experimental group received intragastric administration of fraxetin (25 mg/kg·d) every three days for a month. In contrast, the control group received intragastric administration of DMSO. Tumor formation in mice was monitored for 30 days, and the length and width were measured every three days. Tumor volume was calculated based on the formula $V = (\text{length} \times \text{width}^2)/2$, where length was always the longest dimension of the tumor. At the end of the experiment, all the mice were euthanized by CO2 asphyxiation. This animal study was approved by the Institutional Animal Care and Use Committee of Wenzhou Medical University, China. The animal experiments were conducted according to all regulatory institutional guidelines for animal welfare (National Institutes of Health Publications, NIH Publications No. 80 − 23) [20].

Histopathological analysis

Tumor specimens from animals embedded in paraffin were cut into 4-μm sections and stained with hematoxylin and eosin (HE, Yuanye Biotechnology, Shanghai, China). Immunohistochemical (IHC) analysis was performed according to a previous report [18]. In brief, 4-μm thick sections were dewaxed with xylene and rehydrated in sequential ethanol. Sections were incubated in 0.1% sodium citrate buffer (pH 6.0) for antigen retrieval, and endogenous peroxidase activity was blocked with 3% hydrogen peroxide (Beyotime). IHC staining was performed using the following primary antibodies: anti-Ki67 (1:200, Abcam) and anti-E-cadherin (1:200, Abcam). The integrated optical density (IOD) was measured using Image-Pro Plus software (version 6.0, Media Cybernetics, Silver Spring, MD, USA). All samples were semi-quantitatively or quantitatively assessed by two independent investigators in a blinded manner.

Western blot analysis

Whole proteins from the normal pancreatic ductal cell (hTERT-HPEN) and PCCs (PANC-1, Patu8988 and BxPc-3) or PDA tissues treated with fraxetin for 24 h were collected and protein concentrations were determined by double star choline acid protein analysis kit (Beyotime). Total protein (20 μg) of each sample was separated by SDS-PAGE and then was transferred to a polyvinylidene difluoride membrane (PVDF, Solarbio, Beijing, China). After blocking the membranes for 1 h at room temperature with 5% skim nonfat milk, membranes were incubated with the primary antibodies (1:1000), including anti-caspase-3 (Proteintech, Wuhan, China), anti-caspase-8 (Proteintech), anti-Bcl-2 (Proteintech), anti-Bax (Proteintech), anti-N-cadherin (Abcam), anti-Slug (Abcam), anti-JAK2 (Abcam), anti-p-JAK2 (Abcam), anti-STAT3 (CST), anti-p-STAT3 (CST), anti-E-cadherin (Abcam), anti-type Ⅳ collagen (Abcam), anti-GLUT1 (Affinity Biosciences, Cincinnati, OH, USA), anti-VEGFA (Affinity), anti-HIF-1α (Affinity), anti-Ref1 (Abcam), and anti-vimentin (Abcam), overnight at 4 ℃. After washing in TBST (10 mM Tris-HCl, 150 mM NaCl and 0.1% Tween-20), membranes were incubated with secondary antibodies (1:400) for 1 h at room temperature.

Finally, the protein bands were visualized using chemiluminescence detection on autoradiographic film and the GADPH antibody (1:8000, Proteintech) was used as the internal reference.

ROS level assay

ROS level assay was performed according to the manufacturer's instructions (Beyotime). In brief, PANC-1 or Patu8988 cells were seeded in a 6-well plate with a density of about 5×10^4/well. After the cells adhere to the wall, cells were treated with fraxetin for 24 h. On the second day, 2 ml of the dilution (DCFH-DA, 1:1000, Beyotime) was added to each well, incubated at 37 ℃ for 30 min, and then the cells were collected. Images were captured using a fluorescence microscope (Leica Microsystems). In addition, the cells were also resuspended in PBS, and ROS level was detected by flow cytometry (BD Biosciences).

Database analysis

The expression of STAT3 in PDA tissues and adjacent normal tissues in the GEPIA 2 database website (http://gepia2.cancer-pku.cn/#analysis) was analyzed. Besides, the correlation between STAT3 expression and KRAS activity was also evaluated in the GEPIA 2 database. Moreover, the potential target candidates were analyzed using the PharmMapper Server (http://www.lilab-ecust.cn/pharmmapper/index.html) according to a previous report [21].

Molecular docking

Fraxetin structure was downloaded from PubChem (https://pubchem.ncbi.nlm.nih.gov) as SDF files and converted into mol2 format using Chimera. The STAT3 crystal structure was downloaded from PDB no. 6NJS as a model (http://www.rcsb.org). Compound and protein were converted into PDBQT format using AudoDockTools and docked using AutoDock Vina. Visualize conformations and interactions were prepared by PyMol, Chimera, and LigPlot+.

Statistical analysis

Data were presented as the means ± standard deviations. All statistical analyses were performed using GraphPad Prism software (version 8.0, GraphPad Software, Inc., La Jolla, CA, USA). A two-sided Student's t-test was used to analyze differences between the two groups. One-way analysis of variance (ANOVA) with Bonferroni's post-hoc test was used when more than two groups were present. $P < 0.05$ was considered statistically significant.

Results

Fraxetin inhibits cellular proliferation and induces mitochondrial-dependent apoptosis in PCCs

To investigate the effects of fraxetin on PCC proliferation, unlabeled real-time cell analysis (RTCA), CCK-8 assay and colony formation assay were performed. As shown in Fig. 1B, the viability of PANC-1 cells incubated for 24 h gradually decreased when the concentration of fraxetin (0 ~ 200 μM) gradually

increased in a concentration-dependent manner. Similarly, CCK-8 results of Patu8988 cells also confirmed the concentration-dependent effects of fraxetin (Fig. 1B), especially when the concentration of fraxetin is 25 ~ 100 μM. Thus, we selected 50 and 100 μM of fraxetin for subsequent anti-proliferative studies. Based on the RTCA results, the growth of PANC-1 and Patu8988 cells was markedly inhibited by fraxetin treatment, and it was time-dependent (Fig. 1C). Moreover, fraxetin significantly reduced the number of colony formation in PANC-1 and Patu8988 cells (Fig. 1D). These results supported the anti-proliferative activity of fraxetin in PCCs.

A previous study has shown that Ki67 (also known as MKI67) is a cellular marker for proliferation and is highly expressed in PDA tissues [22]. Ki67 is present during all active phases of the cell cycle (G1, S, G2 and M), but is absent in resting cells (G0) and the cellular content of Ki67 protein markedly increases during PCC progression through the S phase of the cell cycle [23]. In this study, the ratio of Ki67-positive cells in total cells was reduced in fraxetin-treated PANC-1 and Patu8988 cells compared with the control (Fig. 1E). Taken together, these results suggested that fraxetin has proliferation-inhibitory activities on PCCs and it is time- and concentration-dependent.

Given fraxetin has anti-proliferative activity in PCCs, whether fraxetin can induce cellular apoptosis. The apoptotic PCCs were examined by flow cytometry to detect labeled Annexin V-FITC/PI. As expected, we found that fraxetin concentration-dependently increased the ratio of early apoptotic cells but also enhanced the ratio of late apoptotic and necrotic cells (Fig. 1F). Caspases, a family of cysteine proteases, are the central regulators of apoptosis. As a key protease, caspase-3 is cleaved and activated during the early stage of apoptosis to execute apoptosis by cleaving targeted cellular proteins [24]. In this study, the expression of cleaved caspase-3 was upregulated by fraxetin treatment (Fig. 1G). Besides, fraxetin also increased the expression of cleaved caspase-8 (Fig. 1G), which can be used as an apoptotic initiator to activate caspase-3 [25]. Moreover, enhanced Bax expression and reduced Bcl-2 expression in fraxetin-treated PANC-1 and Patu8988 cells were observed (Fig. 1G). Collectively, these findings indicated that fraxetin induces apoptosis of PCCs through a mitochondrial-dependent pathway.

Fraxetin inhibits PCC invasion and migration via Slug-E-cadherin-dependent EMT

Next, we evaluated the effects of fraxetin on the invasion and migration of PCCs by transwell invasion and wound healing assay. As shown in Fig. 2A, in PANC-1 and Patu8988 cells, fraxetin treatment significantly reduced the number of invasive cells in a concentration-dependent manner. In addition, the migration of PANC-1 and Patu8988 cells was inhibited by fraxetin, and it is time- and concentration - dependent (Fig. 2B). Further study showed that the suppressive effect of fraxetin on the invasion and migration of PCCs might be related to the inhibition of epithelial-mesenchymal transition (EMT). EMT is a developmental process that plays an important role in PDA progression and metastasis [26]. The EMT is characterized by the loss of cell-to-cell adhesion and is associated with the phenotypic conversion of epithelial cells into mesenchymal-like cells [27]. E-cadherin is the major adhesion protein associated with epithelial cells and is considered an active suppressor of invasion and growth of PDA [28]. Currently, EMT-

associated transcription factor Slug (Snail2), a member of the Snail superfamily, is known to directly bind to the E-boxes of E-cadherin gene promoter and repress its transcription [29]. Thus, we evaluated the expression of E-cadherin and Slug in fraxetin-treated PCCs. E-cadherin expression was enhanced in PANC-1 and Patu8988 cells upon fraxetin treatment (Fig. 2C,D). In addition, fraxetin decreased the expression of matrix components, including α-SMA, N-cadherin and Vimentin (Fig. 2C,D). Moreover, fraxetin reduced Slug expression (Fig. 2C). Thus, these data reveal an inhibitory effect of fraxetin on the invasion and migration of PCCs by regulating the EMT process dependent on the Slug-E-cadherin axis.

Fraxetin inhibits tumor growth and metastasis of PDA in animal xenograft models

Given fraxetin inhibited the proliferation, migration and invasion, and induced apoptosis of PANC-1 and Patu8988 cells *in vitro*, whether the similar anti-tumor mechanism of fraxetin occurred in nude mice of PDA xenografts *in vivo*. Fraxetin (25 mg/kg·d) was administered continuously for 30 days to the mice subjected to the injection of PCCs. Figure 3A showed morphologic changes in the experimental groups as a result of fraxetin treatment. We found that fraxetin administration significantly reduced the volume and weight of the tumor (Fig. 3B,C). Evidence from HE-staining showed PDA pathological results in tissues of the model group (Fig. 3D). In addition, the decreased proportion of Ki67-positive cells in total cells in fraxetin-treated models showed the inhibition of tumor cell proliferation (Fig. 3E). Further studies showed that fraxetin administration enhanced the expression of cleaved caspase-8 and cleaved caspase-3 (Fig. 3F,G). Moreover, fraxetin upregulated Bax expression and downregulated Bcl-2 expression (Fig. 3F,G). Thus, our *in vivo* experiments showed that fraxetin induced PCC apoptosis in a mitochondrial-mediated manner.

To access whether fraxetin suppressed PDA metastasis, we examined the expression of EMT-related proteins. Immunohistochemical analysis showed that fraxetin significantly increased E-cadherin expression (Fig. 3H). The enhanced expression of E-cadherin was confirmed by Western Blot results (Fig. 3I,J). Furthermore, fraxetin reduced the expression of Slug expression (Fig. 3I,J). Thus, fraxetin inhibited PDA metastasis in animal xenograft models via Slug-E-cadherin-dependent EMT.

Fraxetin enhanced the sensitivity of PCCs to gemcitabine

Gemcitabine is currently the first-line drug for PDA chemotherapy, but chemotherapy resistance is widespread and has become the main reason for the failure of PDA chemotherapy [30]. Therefore, it is crucial to inhibit gemcitabine resistance and promote its anti-PDA efficacy. Here, evidence from colony formation assay showed that gemcitabine has a certain inhibitory effect on the proliferation of PCCs, and this effect can be enhanced by fraxetin (Fig. 4A,B). Besides, fraxetin treatment also strengthens the inhibitory effects of gemcitabine on the infiltration and invasion of PCCs (Fig. 4C-F) by downregulating N-cadherin expression and upregulating Vimentin expression (Fig. 4G,H). Thus, these findings indicated that fraxetin could enhance the sensitivity of PCCs to the chemotherapy drug gemcitabine.

Fraxetin induced STAT3 inactivation by occupying its SH2 domain in vitro and in vivo

A previous study has shown that STAT3 is involved in fraxetin-mediated inhibition in the proliferation of lung cancer cells [17]. In PDA, KRAS mutation, including G12D and G12V, drives STAT3 activation [13], which was consistent with our conclusion (Fig. 5A-C). Moreover, over-activation of STAT3 induces the chemoresistance of PCCs to the chemotherapy drug gemcitabine [31]. Thus, we hypothesized that fraxetin exerts its protective effects by targeting STAT3 activity in PANC-1 (KRAS G12D) and Patu8988 (KRAS G12V) cells. Although there was no significant difference in the expression of JAK2 and STAT3 protein between the fraxetin-treated group and the control group, the phosphorylation levels of JAK2 (Y1007) and STAT3 (Y705) were significantly suppressed by fraxetin treatment (Fig. 5D). Considering that the activation of STAT3 is due to the nuclear expression of phosphorylated STAT3, we detected the nuclear localization of STAT3 by immunocytochemical staining. The results showed that the nuclear expression of STAT3 in PANC-1 and Patu8988 cells was inhibited by fraxetin (Fig. 5E). Furthermore, in animal xenograft models, fraxetin administration suppressed the phosphorylation of JAK2 and STAT3 (Fig. 5F). Taken together, our *in vitro* and *in vivo* experiments showed that inhibition of STAT3 activity might be critical for fraxetin-mediated anti-tumor effects in PDA.

Next, we analyzed the interaction between fraxetin and STAT3 protein. As shown in Fig. 5G, the STAT3 protein harbor conserved motifs, including Src Homology 2 (SH2) domain. We found that there are interactions between fraxetin and protein residues of STAT3 (6NJS) crystal structure (Fig. 5H). Fraxetin shows important interactions with STAT3 SH2 domain residues (Fig. 5I). It makes hydrogen bonds (green dotted line) with Arg609, Ser611, glu612, Ser613, Thr620 and Val637 residues (Fig. 5I,J). It also creates a favorable group of a hydrophobic pocket (red symbol) formed by Ser636, Glu638 and Pro639 (Fig. 5J). As a result, fraxetin has placed at the centre SH2 domain to occupy the pTyr-recognition site of its SH2 domain of another STAT3 monomer, thereby preventing its homo-dimer formation, which then inhibits the phosphorylation of STAT3 and blocks the activation of STAT3-downstream signaling pathways.

Reactivation of STAT3 reverses the anti-tumor effects of fraxetin in PDA

Since fraxetin exerts its protective effects on PDA by targeting STAT3 activity, whether reactivation of STAT3 can rescue the inhibitory effects of fraxetin. In this study, colivelin, a neuroprotective peptide with brain permeability, was used to activate STAT3 [32]. Firstly, evidence from colony formation assay showed that colivelin increased the number of colonies, revealing that reactivated STAT3 relieved fraxetin-mediated inhibition of PCC proliferation (Fig. 6A). In addition, colivelin enhanced the number of invasive cells in fraxetin-treated PANC-1 and Patu8988 cells, indicating that colivelin-induced overactivation of STAT3 reversed fraxetin-mediated inhibition of PCC invasion (Fig. 6B). Furthermore, the ability of cell mobility in fraxetin-treated PANC-1 and Patu8988 cells was strengthened by colivelin treatment, suggesting that upregulated STAT3 activity by colivelin abolished the inhibition of PCC migration caused by fraxetin (Fig. 6C). Thus, these results confirmed again that reactivation of STAT3 by

colivelin enhances the biological behavior of PCCs upon fraxetin treatment, and the STAT3 is crucial for the inhibitory effect of fraxetin on PDA.

Next, we evaluated the effects of STAT3 reactivation on the EMT. In fraxetin-treated PANC-1 and Patu8988 cells, colivelin reduced E-cadherin expression, as determined by Western blot and immunocytochemical staining (Fig. 6D,E), revealing that epithelial phenotypic features are suppressed by reactivation of STAT3. Further study showed that Slug expression in fraxetin-treated PANC-1 and Patu8988 cells was increased by colivelin treatment (Fig. 6D), thereby indicating that STAT3 reactivation abolished fraxetin-mediated EMT inhibition. Moreover, in fraxetin-treated PANC-1 and Patu8988 cells, colivelin upregulated the expression of N-cadherin and type I collagen (Fig. 6F), as well as vimentin (Fig. 6G), suggesting that STAT3 reactivation induced excessive accumulation of matrix. Collectively, STAT3 reactivation by colivelin reverses the anti-tumor effects of fraxetin on PDA.

Fraxetin inhibited angiogenesis, glucose metabolism and EMT in PCCs

To further clarify the mechanism by which fraxetin exerts its protective effects on PDA by inhibiting STAT3 activation, we analyzed the expression and release of downstream target molecules of this signaling. STAT3 downstream molecules, including Bcl-2, E-cadherin, hypoxia-inducible factor-1α (HIF-1α), and vascular endothelial growth factor-α (VEGFA), are involved in the regulation of cellular proliferation, apoptosis, angiogenesis, and metastasis [10, 33]. As mentioned before, reduced Bcl-2 expression in fraxetin-treated PCCs indicated mitochondrial pathway-dependent apoptosis (Fig. 1G). Also, fraxetin inhibits the EMT process by blocking the Slug-E-cadherin axis (Fig. 2C,D). In addition to these, fraxetin-mediated downregulation in the expression levels of HIF-1α and VEGFA revealed the inhibition of hypoxia-induced angiogenesis (Fig. 7A-C). Moreover, the levels of oxygen consumption rate (OCR) in PANC-1 and Patu8988 cells were downregulated by fraxetin treatment by inhibiting basal respiration, spare respiration, maximal respiration, and ATP production (Fig. 7D-G). The levels of extracellular acidification rate (ECAR) were decreased by fraxetin by antagonizing basal glycolysis and compensatory glycolysis (Fig. 7H-K). Importantly, reduced expression of glucose transporter type 1 (GLUT1), a uniporter protein that facilitates the transport of glucose across the plasma membranes of mammalian cells for metabolism [34], in fraxetin-treated PCCs was responsible for the reduction of glucose metabolism (Fig. 7L). Thus, these findings indicated that in PDA fraxetin hinders hypoxia-induced angiogenesis by decreasing the expression levels of HIF-1α and VEGFA, controls glucose uptake and metabolism by reducing GLUT1 expression, and inhibits the EMT by blocking the Slug-E-cadherin axis.

Fraxetin drove ROS-mediated apoptosis by regulating STAT3-Ref1 axis

As mentioned above, fraxetin induces cell apoptosis via Bcl-2-mediated mitochondrial pathway. In PDA, Bcl-2 expression can be regulated by ROS [35]. In this study, we found that the levels of ROS were significantly increased in fraxetin-treated PCCs (Fig. 8A-C), suggesting that fraxetin-induced apoptosis

might be mediated by ROS. Further study revealed that downregulated Ref1 expression was involved in ROS-triggered apoptosis of PCCs when exposed to fraxetin (Fig. 8D,E). Ref1 is an important target molecule of STAT3 that can regulate ROS levels [36]. We also found that Ref1 expression was positively associated with STAT3 activity in PDA (Fig. 8F). Reactivation of STAT3 with colivelin abolished fraxetin-induced downregulation of Ref1 expression in PDA (Fig. 8G). Thus, these results indicated that fraxetin drove ROS-mediated apoptosis by regulating the STAT3-Ref1 axis.

Discussion

In the present study, we investigated for the first time the anti-tumor effects of fraxetin on pancreatic ductal adenocarcinoma (PDA) *in vitro* and *in vivo*. In pancreatic cancer cells (PCCs), fraxetin inhibited cell proliferation by downregulating Ki67 expression. In addition, fraxetin induced PCC apoptosis through the mitochondrial-mediated pathway. Moreover, fraxetin suppressed the invasion and migration of PCCs by regulating epithelial-mesenchymal transition (EMT) dependent on the Slug-E-cadherin axis. In nude mouse models, PDA growth and metastasis were reduced by fraxetin treatment. Thus, these evidence supported that fraxetin exerts effective protection against PDA.

PDA, which accounts for over 90% of pancreatic cancer, is an aggressive type of malignant tumor with an overall 5-year survival rate of less than 8% [1]. PDA can be hard to treat surgically due to the location of the organ, and because the disease has often spread in the body by the time it is diagnosed. Thus, developing effective drugs for treating PDA is still needed. Recently, multiple studies show that several natural products may become novel candidate agents for developing PDA therapeutics [37, 38]. Fraxetin is a plant-derived coumarin primarily isolated from *Fraxinus bungeana A.DC.*, and has been reported to exert potent anti-bacterial, neuroprotective and anti-inflammatory effects [14]. In breast cancer cells, fraxetin inhibits cellular proliferation, induces mitochondrial-dependent apoptosis by upregulating Bax expression and downregulating Bcl-2 expression [15]. Also, fraxetin treatment causes a significant cell cycle arrest and pro-apoptotic effects in non-small-cell lung cancer cells [17]. Similar to the above studies, our *in vivo* and *in vitro* experiments also identified anti-tumor effects of fraxetin in PDA by inducing PCC apoptosis, inhibiting proliferation, and reducing tumor growth. Moreover, fraxetin prevented PDA progression by suppressing the invasion and migration of PCCs. Thus, our results provide a rationale for the use of fraxetin as a potential supplemental treatment for PDA.

Interestingly, we found that fraxetin can enhance the sensitivity of PCCs to the chemotherapy drug gemcitabine. Gemcitabine is accepted as the standard treatment for patients with locally or metastatic advanced PDA, but the problem of its drug resistance has become increasingly prominent [39]. How to solve the weakening of its anti-tumor effect due to drug resistance is an important task now. For this reason, drugs such as human recombinant hyaluronidase (PEGPH20) or CD40 monoclonal antibody (CP-870,893) have entered clinical studies to increase the efficacy of gemcitabine against advanced PDA [40, 41]. Our results identified fraxetin as an adjuvant drug to strengthen the anti-tumor effect of gemcitabine by inhibiting the EMT and PCC proliferation. Therefore, fraxetin may be a potential drug development candidate for PDA treatment.

Further studies have shown that STAT3 activity is responsible for fraxetin-mediated anti-tumor effects [11–13]. Although STAT3 is dispensable for the development of the pancreas, the majority of PDA show constitutive activation of STAT3 by phosphorylation at Y705 and induction into the nucleus [13]. Importantly, STAT3 activation is mainly driven by oncogenic KRAS mutation, which is found in ~ 95% of pancreatic intraepithelial neoplasias (PanINs), the earliest pre-neoplastic stages of PDA progression [13, 42, 43]. Thus, targeted inhibition of STAT3 might be a potential therapeutic strategy for PDA. AG-409, a tyrosine kinase inhibitor that inhibits STAT3 activation, decreased the invasion and metastasis ability of PDA [44]. In addition, novel small-molecule STAT3 inhibitors FLLL31 and FLLL32, which are derived from curcumin, inhibited multiple oncogenic processes and induced apoptosis in PCC lines, and reduced tumor growth and vascularity in PDA mouse xenografts [45]. Our findings also supported STAT3 as a key target for the anti-tumor activity of fraxetin. Fraxetin treatment not only inhibited the phosphorylation (Y1007) of JAK2 in PCCs, but also antagonized the phosphorylation (Y705) and nuclear localization of STAT3. Furthermore, reactivating STAT3 with colivelin relieved fraxetin-mediated induction of apoptosis, and inhibition of proliferation, invasion and migration of PCCs, thereby enhancing the biological behavior of PCCs upon fraxetin treatment.

Importantly, fraxetin antagonized the phosphorylation (Y705) of STAT3 protein by direct interaction. Fraxetin binds to STAT3 SH2 domain residues by hydrogen bonding with Arg609, Ser611, glu612, Ser613, Thr620 and Val637 residues. It also creates a favorable group of a hydrophobic pocket formed by Ser636, Glu638 and Pro639. Thus, fraxetin occupies the pTyr-recognition site of STAT3 SH2 domain to prevent its homo-dimer formation, and thereby suppresses the phosphorylation of STAT3 and blocks the activation of STAT3-downstream signal pathways.

In PDA initiation and development, STAT3 exerts its important physiological function through a series of downstream target molecules. The STAT3-downstream molecules, including Bcl-2, E-cadherin, HIF-1α, and VEGFA, play key roles in the regulation of proliferation, apoptosis, angiogenesis, and metastasis of PCCs [10, 33]. E-cadherin is a calcium-dependent cell adhesion protein involved in mechanisms regulating cell-cell adhesion and mobility of epithelial cells [46, 47]. Loss of intercellular adhesion and increased cell motility promotes tumor cell invasion and migration through EMT [48]. In the hypoxic microenvironment of PDA, HIF-1α is crucial for angiogenesis by inducing VEGFA expression [49]. In addition, enhanced HIF-1α activity in PDA promotes glycolysis by regulating GLUT1 expression in PCCs [50]. Our findings indicated that fraxetin reduced Bcl-2 expression and thereby induced mitochondrial-dependent apoptosis in PCCs. Also, fraxetin inhibited the EMT process by blocking the Slug-E-cadherin axis. Moreover, fraxetin hindered hypoxia-induced angiogenesis by decreasing the expression levels of HIF-1α and VEGFA, controlled glucose uptake and metabolism by reducing GLUT1 expression. Importantly, reactivation of STAT3 with colivelin reversed fraxetin-mediated inhibition of EMT via the Slug-E-cadherin axis. These evidence supported a crucial role of STAT3 in fraxetin-mediated anti-tumor effects again.

In addition to the direct regulation of Bcl-2 expression by STAT3, we also found that fraxetin-induced apoptosis was mediated indirectly by ROS. ROS triggers mitochondrial apoptosis pathway by regulating Bcl-2 expression [35]. Further study revealed that reduced Ref1 expression contributed to ROS-triggered

apoptosis of PCCs when exposed to fraxetin. As a target molecule of STAT3, Ref1 plays an important role in the regulation of ROS levels and oxidative stress [36]. Colivelin was used to reactivate STAT3 and thereby resulted in the abolishment of fraxetin-induced downregulation of Ref1 expression in PDA. These results indicated that fraxetin drove ROS-mediated apoptosis by regulating the STAT3-Ref1 axis.

However, there exist some apparent limitations. First, a genetic approach to evaluate the role of STAT3 in fraxetin-mediated anti-tumor effects needs to be presented. In addition, the mechanism of KRAS-mutation (G12D or G12V) affects the anti-tumor effects of fraxetin should be clarified. It is also worth mentioning that the anti-tumor potential of fraxetin in clinical application, including pharmacokinetics and its side effects, needs to be further clarified.

Conclusions

Fraxetin inhibited PCC proliferation, induced mitochondrial-mediated apoptosis, and suppressed the invasion and migration by regulating EMT. In nude mouse models, PDA growth and metastasis were reduced by fraxetin treatment. Moreover, fraxetin strengthens the anti-tumor effect of gemcitabine by inhibiting PCC proliferation and EMT. Mechanically, oncogenic KRAS-triggered STAT3 activation in PCCs and PDA tissues was suppressed by fraxetin via occupying STAT3 SH2 domain. Consequently, fraxetin hindered hypoxia-induced angiogenesis by decreasing HIF-1α and VEGFA expression, controlled glucose metabolism by reducing GLUT1 expression, inhibited the EMT by blocking the Slug-E-cadherin axis, and drove ROS-mediated apoptosis by regulating STAT3-Ref1 axis. Reactivation of STAT3 reverses the anti-tumor effects of fraxetin (Fig. 9). Thus, pharmacological inhibition of STAT3 activity with fraxetin suppresses oncogenesis and development of PDA by antagonizing STAT3 activation, and fraxetin can be a *therapeutic* approach to PDA.

Abbreviations

2-DG, 2-Deoxyglucose 2-Deoxyglucose; Bax, Bcl-2-associated X protein; Bcl-2, B-cell lymphoma 2; CCK-8, cell counting kit 8; DAPI, 4'6-diamidino-2-phenylindole; ECAR, extracellular acidification rate; EMT, epithelial-mesenchymal transition; FCCP, Carbonyl cyanide 4-(trifluoromethoxy) phenylhydrazone; GAPDH, glyceraldehyde 3-phosphate dehydrogenase; GLUT1, glucose transporter type 1; HIF-1α: hypoxia-inducible factor-1α; JAK2, Janus kinase 2; ROS, reactive oxygen species; OCR, oxygen consumption rate; PCC, pancreatic cancer cell; PDA, pancreatic ductal adenocarcinoma; RTCA, real-time cell analysis; SH2, Src Homology 2; STAT3, signal transducer and activator of transcription 3; VEGFA: vascular endothelial growth factor-α

Declarations

Ethics approval and consent to participate

All animal studies were performed with an approved protocol by the Institutional Animal Care and Use Committee of Wenzhou Medical University.

Consent for publication

The authors declare that they agree to submit the article for publication.

Availability of data and materials

The datasets used and/or analyzed during the current study are available from the corresponding author on reasonable request.

Competing interests

The authors declare that they have no competing interests.

This study was sponsored by Wenzhou Science and Technology Plan Project, China (Grant No. Y20180100) and Key Laboratory of Diagnosis and Treatment of Severe Hepato-Pancreatic Diseases of Zhejiang Province (Grant No. 2018E10008).

Authors' contributions

YB and QZ designed the research. YG, HG and DC performed the experiments, analyzed the data and drafted the manuscript. YX, HZ, ZX, and JL performed the experiments and collected data for the revision. YG and YB edited the manuscript. YG, JW, JD, XL, and YB contributed to the discussion and review of the manuscript.

Acknowledgements

We thank Dr. Tongke Chen (the Experimental Animal Center of Wenzhou Medical University, Wenzhou, China) for technical assistance for animal experiments.

Authors' information

[1]Key Laboratory of Diagnosis and Treatment of Severe Hepato-Pancreatic Diseases of Zhejiang Province, The First Affiliated Hospital of Wenzhou Medical University, Wenzhou 325000, China; [2]The Sixth People's Hospital of Wenzhou City, Wenzhou 325000, China; [3]Engineering Research Center of Clinical Functional Materials and Diagnosis & Treatment Devices of Zhejiang Province, Wenzhou Institute, University of Chinese Academy Sciences, Wenzhou 325000, China; [4]State Key Laboratory of Cellular Stress Biology, Innovation Center for Cell Signaling Network, School of Life Sciences, Xiamen University, Xiamen, Fujian, China; [5]Platform for Radiation Protection and Emergency Preparedness, School of Public Health and Management, Wenzhou Medical University, Wenzhou 325000, China; [6]Center for Health Assessment, Wenzhou Medical University, Wenzhou, 325000, China; [7]Department for Hepatopancreatobiliary Surgery, The First Affiliated Hospital of Wenzhou Medical University, Wenzhou, 325000, China

References

1. Bray F, Ferlay J, Soerjomataram I, Siegel RL, Torre LA, Jemal A. Global cancer statistics 2018: GLOBOCAN estimates of incidence and mortality worldwide for 36 cancers in 185 countries. CA

Cancer J Clin. 2018;68:394-424.

2. Lee HS, Jang CY, Kim SA, Park SB, Jung DE, Kim BO, Kim HY, Chung MJ, Park JY, Bang S, et al. Combined use of CEMIP and CA 19-9 enhances diagnostic accuracy for pancreatic cancer. Sci Rep. 2018;8:3383.
3. Zhang Z, Liu M, Hu Q, Xu W, Liu W, Sun Q, Ye Z, Fan G, Xu X, Yu X, et al. FGFBP1, a downstream target of the FBW7/c-Myc axis, promotes cell proliferation and migration in pancreatic cancer. Am J Cancer Res. 2020;9:2650-64.
4. Zhang X, Lu H, Hong W, Liu L, Wang S, Zhou M, Chen B, Bai Y. Tyrphostin B42 attenuates trichostatin A-mediated resistance in pancreatic cancer cells by antagonizing IL-6/JAK2/STAT3 signaling. Oncol Rep. 2018;39:1892-900.
5. Sansone P, Bromberg J. Targeting the interleukin-6/Jak/stat pathway in human malignancies. J Clin Oncol. 2012;30:1005-14.
6. Bagratuni T, Mavrianou N, Gavalas NG, Tzannis K, Arapinis C, Liontos M, Christodoulou MI, Thomakos N, Haidopoulos D, Rodolakis A, et al. JQ1 inhibits tumour growth in combination with cisplatin and suppresses JAK/STAT signalling pathway in ovarian cancer. Eur J Cancer. 2020;126:125-35.
7. Gao Y, Luo L, Xie Y, Zhao Y, Yao J, Liu X. PYCR1 knockdown inhibits the proliferation, migration, and invasion by affecting JAK/STAT signaling pathway in lung adenocarcinoma. Mol Carcinog. 2020;59:503-11.
8. Jiang L, Zhao XH, Mao YL, Wang JF, Zheng HJ, You QS. Long non-coding RNA RP11-468E2.5 curtails colorectal cancer cell proliferation and stimulates apoptosis via the JAK/STAT signaling pathway by targeting STAT5 and STAT6. J Exp Clin Cancer Res. 2019;38:465.
9. Tsai WC, Bai LY, Chen YJ, Chu PC, Hsu YW, Sargeant AM, Weng JR. OSU-A9 inhibits pancreatic cancer cell lines by modulating p38-JAK-STAT3 signaling. Oncotarget. 2017;8:29233-46.
10. Owen KL, Brockwell NK, Parker BS. JAK-STAT Signaling: A Double-Edged Sword of Immune Regulation and Cancer Progression. Cancers (Basel). 2019;11:2002.
11. Biffi G, Oni TE, Spielman B, Hao Y, Elyada E, Park Y, Preall J, Tuveson DA. IL1-Induced JAK/STAT Signaling Is Antagonized by TGFbeta to Shape CAF Heterogeneity in Pancreatic Ductal Adenocarcinoma. Cancer Discov. 2018;9:282-301.
12. Chen L, Zhou D, Liu Z, Huang X, Liu Q, Kang Y, Chen Z, Guo Y, Zhu H, Sun C. Combination of gemcitabine and erlotinib inhibits recurrent pancreatic cancer growth in mice via the JAK-STAT pathway. Oncol Rep. 2018;39:1081-9.
13. Corcoran RB, Contino G, Deshpande V, Tzatsos A, Conrad C, Benes CH, Levy DE, Settleman J, Engelman JA, Bardeesy N. STAT3 plays a critical role in KRAS-induced pancreatic tumorigenesis. Cancer Res. 2011;71:5020-9.
14. Zhao CN, Yao ZL, Yang D, Ke J, Wu QL, Li JK, Zhou XD. Chemical Constituents from Fraxinus hupehensis and Their Antifungal and Herbicidal Activities. Biomolecules. 2020;10:74.

15. Liu G, Liu Z, Yan Y, Wang H. Effect of fraxetin on proliferation and apoptosis in breast cancer cells. Oncol Lett. 2018;14:7374-8.
16. Sanchez-Reus MI, Peinado, II, Molina-Jimenez MF, Benedi J. Fraxetin prevents rotenone-induced apoptosis by induction of endogenous glutathione in human neuroblastoma cells. Neurosci Res. 2005;53:48-56.
17. Zhang Y, Wang L, Deng Y, Zhao P, Deng W, Zhang J, Luo J, Li R. Fraxetin Suppresses Proliferation of Non-Small-Cell Lung Cancer Cells via Preventing Activation of Signal Transducer and Activator of Transcription 3. Tohoku J Exp Med. 2019;248:3-12.
18. Deer EL, Gonzalez-Hernandez J, Coursen JD, Shea JE, Ngatia J, Scaife CL, Firpo MA, Mulvihill SJ. Phenotype and genotype of pancreatic cancer cell lines. Pancreas. 2010;39:425-35.
19. Zhang X, Lu H, Xie S, Wu C, Guo Y, Xiao Y, Zheng S, Zhu H, Zhang Y, Bai Y. Resveratrol suppresses the myofibroblastic phenotype and fibrosis formation in kidneys via proliferation-related signalling pathways. Br J Pharmacol. 2019;176:4745-59.
20. Kilkenny C, Browne WJ, Cuthill IC, Emerson M, Altman DG. Improving bioscience research reporting: the ARRIVE guidelines for reporting animal research. PLoS Biol. 2010;8:e1000412.
21. Wang X, Shen Y, Wang S, Li S, Zhang W, Liu X, et al. PharmMapper 2017 update: a web server for potential drug target identification with a comprehensive target pharmacophore database. Nucleic Acids Res. 2017; 45: W356-W60.
22. Panzuto F, Boninsegna L, Fazio N, Campana D, Pia Brizzi M, Capurso G, Scarpa A, De Braud F, Dogliotti L, Tomassetti P, et al. Metastatic and locally advanced pancreatic endocrine carcinomas: analysis of factors associated with disease progression. J Clin Oncol. 2011;29:2372-7.
23. Foltyn W, Zajecki W, Marek B, Kajdaniuk D, Sieminska L, Zemczak A, Kos-Kudla B. The value of the Ki-67 proliferation marker as a prognostic factor in gastroenteropancreatic neuroendocrine tumours. Endokrynol Pol. 2012;63:362-6.
24. Boice A, Bouchier-Hayes L. Targeting apoptotic caspases in cancer. Biochim Biophys Acta Mol Cell Res. 2020;1867:118688.
25. Keller N, Ozmadenci D, Ichim G, Stupack D. Caspase-8 function, and phosphorylation, in cell migration. Semin Cell Dev Biol. 2018;82:105-17.
26. Jiang Y, Zhan H. Communication between EMT and PD-L1 signaling: New insights into tumor immune evasion. Cancer Lett. 2020;468:72-81.
27. Zheng X, Carstens JL, Kim J, Scheible M, Kaye J, Sugimoto H, Wu CC, LeBleu VS, Kalluri R. Epithelial-to-mesenchymal transition is dispensable for metastasis but induces chemoresistance in pancreatic cancer. Nature. 2015;527:525-30.
28. De Craene B, Berx G. Regulatory networks defining EMT during cancer initiation and progression. Nat Rev Cancer. 2013;13:97-110.
29. Serrano-Gomez SJ, Maziveyi M, Alahari SK. Regulation of epithelial-mesenchymal transition through epigenetic and post-translational modifications. Mol Cancer. 2016;15:18.

30. Xiao BY, Wang BC, Lin GH, Li PC. Efficacy and safety of gemcitabine plus capecitabine in the treatment of advanced or metastatic pancreatic cancer: a systematic review and meta-analysis. Ann Palliat Med. 2020; 9: 1631-42.
31. Zhao T, Jin F, Xiao D, Wang H, Huang C, Wang X, et al. IL-37/ STAT3/ HIF-1alpha negative feedback signaling drives gemcitabine resistance in pancreatic cancer. Theranostics. 2020; 10: 4088-100.
32. Zhao H, Feng Y, Wei C, Li Y, Ma H, Wang X, Cui Z, Jin WN, Shi FD. Colivelin Rescues Ischemic Neuron and Axons Involving JAK/STAT3 Signaling Pathway. Neuroscience. 2019;416:198-206.
33. Li B, Huang C. Regulation of EMT by STAT3 in gastrointestinal cancer (Review). Int J Oncol. 2017;50:753-767.
34. Zhou D, Jiang L, Jin L, Yao Y, Wang P, Zhu X. Glucose Transporter-1 Cooperating with AKT Signaling Promote Gastric Cancer Progression. Cancer Manag Res. 2020;12:4151-60.
35. Bi YL, Min M, Shen W, Liu Y. Genistein induced anticancer effects on pancreatic cancer cell lines involves mitochondrial apoptosis, G0/G1cell cycle arrest and regulation of STAT3 signalling pathway. Phytomedicine. 2018; 39: 10-6.
36. Bhat AA, Lu H, Soutto M, Capobianco A, Rai P, Zaika A, et al. Exposure of Barrett's and esophageal adenocarcinoma cells to bile acids activates EGFR-STAT3 signaling axis via induction of APE1. Oncogene. 2018; 37: 6011-24.
37. Han S, Li X, Xia Y, Yu Z, Cai N, Malwal SR, Han X, Oldfield E, Zhang Y. Farnesyl Pyrophosphate Synthase as a Target for Drug Development: Discovery of Natural-Product-Derived Inhibitors and Their Activity in Pancreatic Cancer Cells. J Med Chem. 2019;62:10867-96.
38. Torres MP, Rachagani S, Purohit V, Pandey P, Joshi S, Moore ED, Johansson SL, Singh PK, Ganti AK, Batra SK. Graviola: a novel promising natural-derived drug that inhibits tumorigenicity and metastasis of pancreatic cancer cells in vitro and in vivo through altering cell metabolism. Cancer Lett. 2012;323:29-40.
39. Frappart PO, Hofmann TG. Pancreatic Ductal Adenocarcinoma (PDAC) Organoids: The Shining Light at the End of the Tunnel for Drug Response Prediction and Personalized Medicine. Cancers (Basel). 2020; 12.
40. Beatty GL, Torigian DA, Chiorean EG, Saboury B, Brothers A, Alavi A, et al. A phase I study of an agonist CD40 monoclonal antibody (CP-870,893) in combination with gemcitabine in patients with advanced pancreatic ductal adenocarcinoma. Clin Cancer Res. 2013; 19: 6286-95.
41. Hingorani SR, Harris WP, Beck JT, Berdov BA, Wagner SA, Pshevlotsky EM, et al. Phase Ib Study of PEGylated Recombinant Human Hyaluronidase and Gemcitabine in Patients with Advanced Pancreatic Cancer. Clin Cancer Res. 2016;22:2848-54.
42. Vincent A, Herman J, Schulick R, Hruban RH, Goggins M. Pancreatic cancer. Lancet. 2011;378:607-20.
43. Kanda M, Matthaei H, Wu J, Hong SM, Yu J, Borges M, Hruban RH, Maitra A, Kinzler K, Vogelstein B, et al. Presence of somatic mutations in most early-stage pancreatic intraepithelial neoplasia. Gastroenterology. 2012;142:730-3 e9.

44. Huang C, Yang G, Jiang T, Huang K, Cao J, Qiu Z. Effects of IL-6 and AG490 on regulation of Stat3 signaling pathway and invasion of human pancreatic cancer cells in vitro. J Exp Clin Cancer Res. 2010;29:51.
45. Lin L, Hutzen B, Zuo M, Ball S, Deangelis S, Foust E, Pandit B, Ihnat MA, Shenoy SS, Kulp S, et al. Novel STAT3 phosphorylation inhibitors exhibit potent growth-suppressive activity in pancreatic and breast cancer cells. Cancer Res. 2010;70:2445-54.
46. Nagathihalli NS, Merchant NB. Src-mediated regulation of E-cadherin and EMT in pancreatic cancer. Front Biosci (Landmark Ed). 2012;17:2059-69.
47. Bai Y, Lu H, Lin C, Xu Y, Hu D, Liang Y, Hong W, Chen B. Sonic hedgehog-mediated epithelial-mesenchymal transition in renal tubulointerstitial fibrosis. Int J Mol Med. 2016;37:1317-27.
48. Zhao T, Jiang W, Wang X, Wang H, Zheng C, Li Y, Sun Y, Huang C, Han ZB, Yang S, et al. ESE3 Inhibits Pancreatic Cancer Metastasis by Upregulating E-Cadherin. Cancer Res. 2016;77:874-85.
49. Bai X, Zhi X, Zhang Q, Liang F, Chen W, Liang C, Hu Q, Sun X, Zhuang Z, Liang T. Inhibition of protein phosphatase 2A sensitizes pancreatic cancer to chemotherapy by increasing drug perfusion via HIF-1α-VEGF mediated angiogenesis. Cancer Lett. 2014;355:281-7.
50. Xi Y, Yuan P, Li T, Zhang M, Liu MF, Li B. hENT1 reverses chemoresistance by regulating glycolysis in pancreatic cancer. Cancer Lett. 2020;479:112-22.

Figures

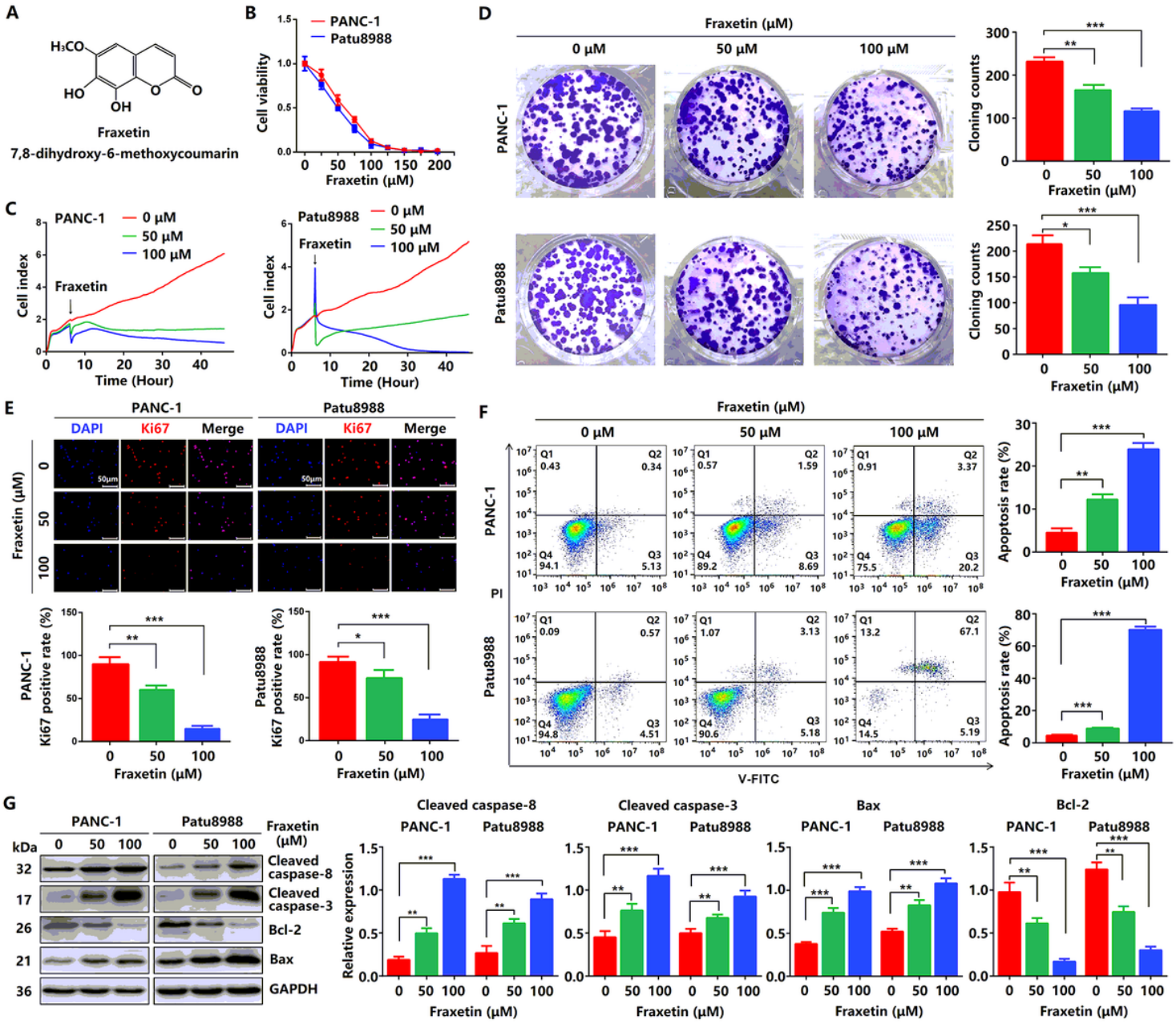

Figure 1

Fraxetin inhibits cellular proliferation and induces mitochondrial-dependent apoptosis in PCCs. (A) The chemical structure of fraxetin. (B) The viability of PANC-1 and Patu8988 cells with or without fraxetin treatment (0~200 μM) was analyzed by CCK-8 assay. (C) The growth of PANC-1 and Patu8988 cells with or without fraxetin treatment was determined by real-time cellular analysis (RTCA). (D) The proliferation of PANC-1 and Patu8988 cells with or without fraxetin treatment was analyzed by colony formation assay. (E) Immunocytochemical staining of Ki67 in PANC-1 and Patu8988 cells with or without fraxetin treatment. Bar = 50 μm. (F) Flow cytometry analysis for cell apoptosis in PANC-1 and Patu8988 cells with or without fraxetin treatment. (G) Western blot analysis showing the expression of cleaved caspase-8, cleaved caspase-3, Bcl-2, and Bax in PANC-1 and Patu8988 cells with or without fraxetin treatment. Data were presented as the mean ± standard deviation, and were analyzed by One-way ANOVA with

Bonferroni's post-hoc test. **P < 0.01, ***P < 0.001. Data were presented as the mean ± standard deviation, and were analyzed by One-way ANOVA with Bonferroni's post-hoc test. *P < 0.05, **P < 0.01, ***P < 0.001.

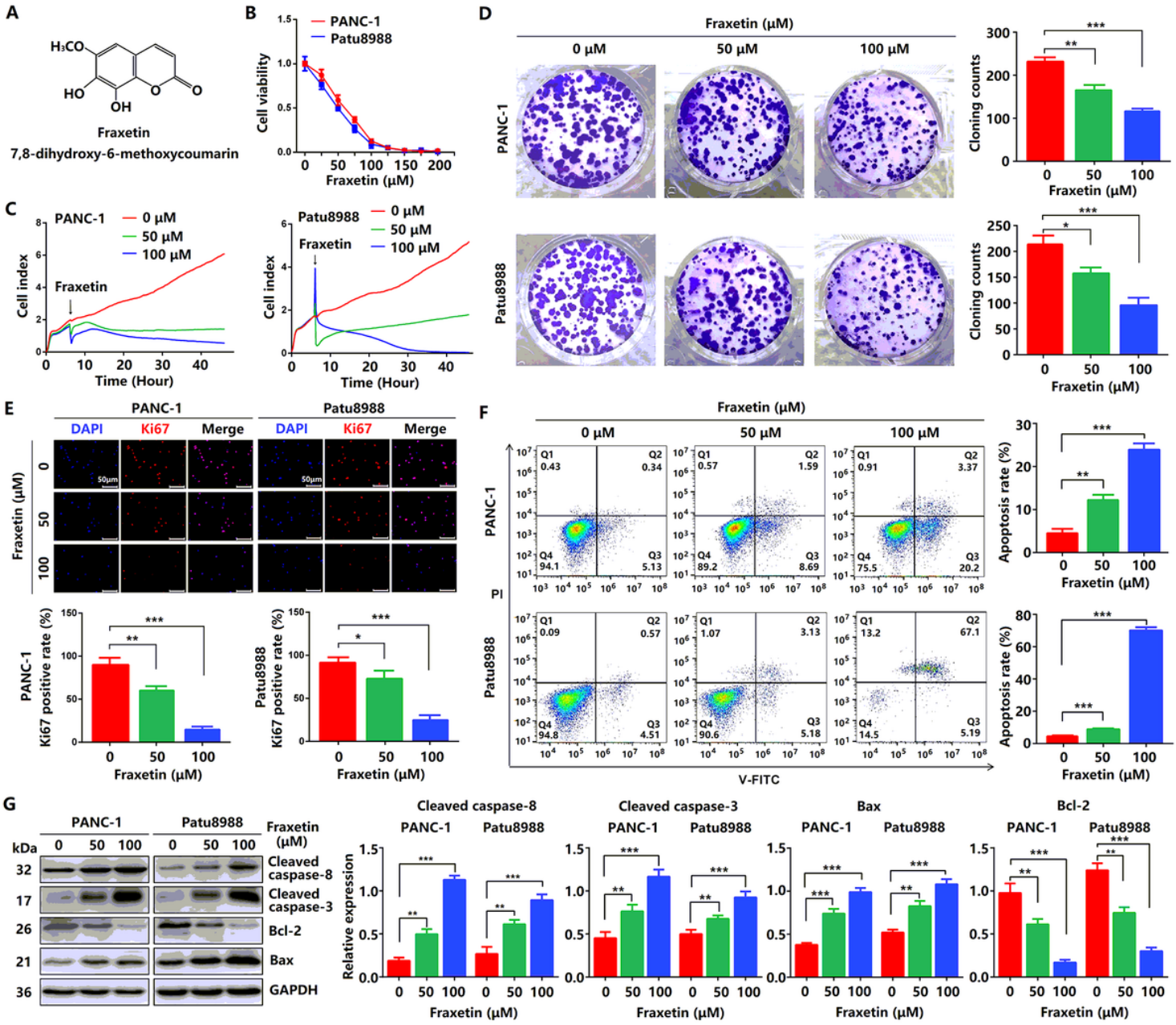

Figure 1

Fraxetin inhibits cellular proliferation and induces mitochondrial-dependent apoptosis in PCCs. (A) The chemical structure of fraxetin. (B) The viability of PANC-1 and Patu8988 cells with or without fraxetin treatment (0~200 μM) was analyzed by CCK-8 assay. (C) The growth of PANC-1 and Patu8988 cells with or without fraxetin treatment was determined by real-time cellular analysis (RTCA). (D) The proliferation of PANC-1 and Patu8988 cells with or without fraxetin treatment was analyzed by colony formation assay. (E) Immunocytochemical staining of Ki67 in PANC-1 and Patu8988 cells with or without fraxetin treatment. Bar = 50 μm. (F) Flow cytometry analysis for cell apoptosis in PANC-1 and Patu8988 cells with

or without fraxetin treatment. (G) Western blot analysis showing the expression of cleaved caspase-8, cleaved caspase-3, Bcl-2, and Bax in PANC-1 and Patu8988 cells with or without fraxetin treatment. Data were presented as the mean ± standard deviation, and were analyzed by One-way ANOVA with Bonferroni's post-hoc test. **P < 0.01, ***P < 0.001. Data were presented as the mean ± standard deviation, and were analyzed by One-way ANOVA with Bonferroni's post-hoc test. *P < 0.05, **P < 0.01, ***P < 0.001.

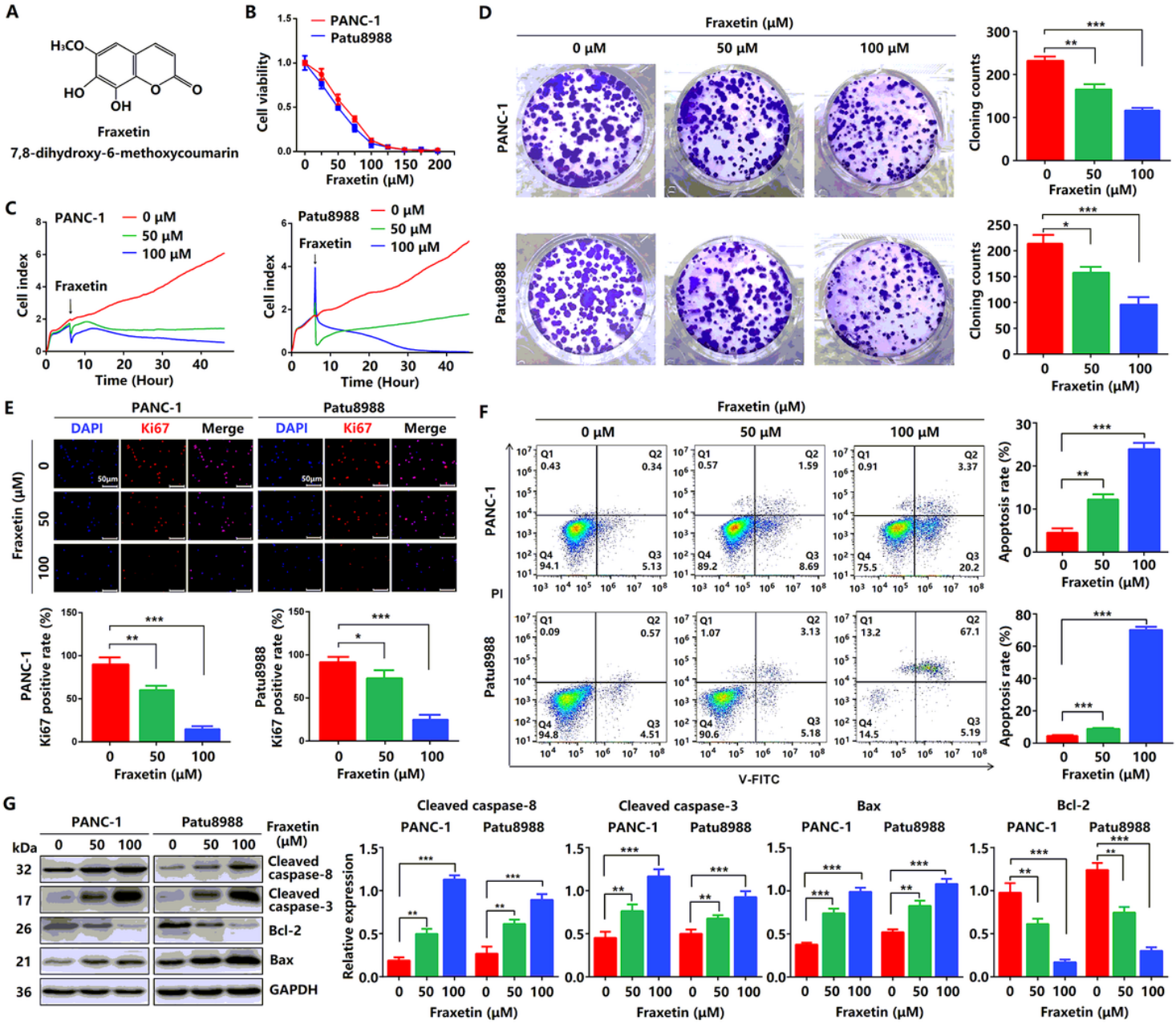

Figure 1

Fraxetin inhibits cellular proliferation and induces mitochondrial-dependent apoptosis in PCCs. (A) The chemical structure of fraxetin. (B) The viability of PANC-1 and Patu8988 cells with or without fraxetin treatment (0~200 μM) was analyzed by CCK-8 assay. (C) The growth of PANC-1 and Patu8988 cells with or without fraxetin treatment was determined by real-time cellular analysis (RTCA). (D) The proliferation

of PANC-1 and Patu8988 cells with or without fraxetin treatment was analyzed by colony formation assay. (E) Immunocytochemical staining of Ki67 in PANC-1 and Patu8988 cells with or without fraxetin treatment. Bar = 50 μm. (F) Flow cytometry analysis for cell apoptosis in PANC-1 and Patu8988 cells with or without fraxetin treatment. (G) Western blot analysis showing the expression of cleaved caspase-8, cleaved caspase-3, Bcl-2, and Bax in PANC-1 and Patu8988 cells with or without fraxetin treatment. Data were presented as the mean ± standard deviation, and were analyzed by One-way ANOVA with Bonferroni's post-hoc test. **P < 0.01, ***P < 0.001. Data were presented as the mean ± standard deviation, and were analyzed by One-way ANOVA with Bonferroni's post-hoc test. *P < 0.05, **P < 0.01, ***P < 0.001.

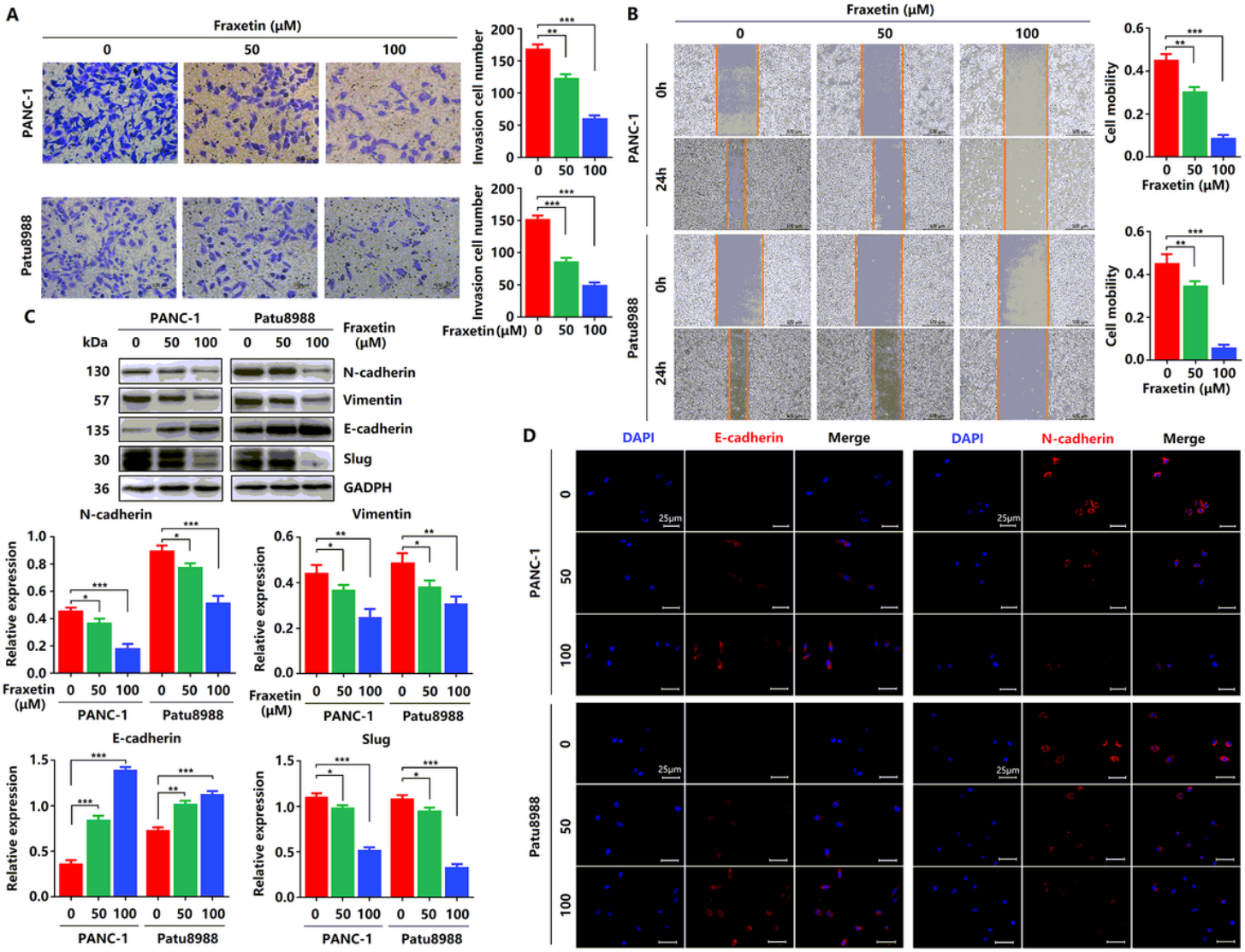

Figure 2

Fraxetin inhibits PCC invasion and migration by regulating the Slug-E-cadherin axis. (A) The effects of fraxetin on the invasion number of PANC-1 and Patu8988 cells were analyzed by transwell chamber assay. (B) The effects of fraxetin on the migrated rate of PANC-1 and Patu8988 cells determined by wound healing assay. (C) Western blot analysis showing the expression of N-cadherin, Vimentin, E-cadherin, and Slug in fraxetin-treated PANC-1 and Patu8988 cells. (D) Immunocytochemical staining of E-

cadherin and α-SMA in fraxetin-treated PANC-1 and Patu8988 cells. Bar = 25 μm. Data were presented as the mean ± standard deviation, and were analyzed by One-way ANOVA with Bonferroni's post-hoc test. *P < 0.05, **P < 0.01, ***P < 0.001.

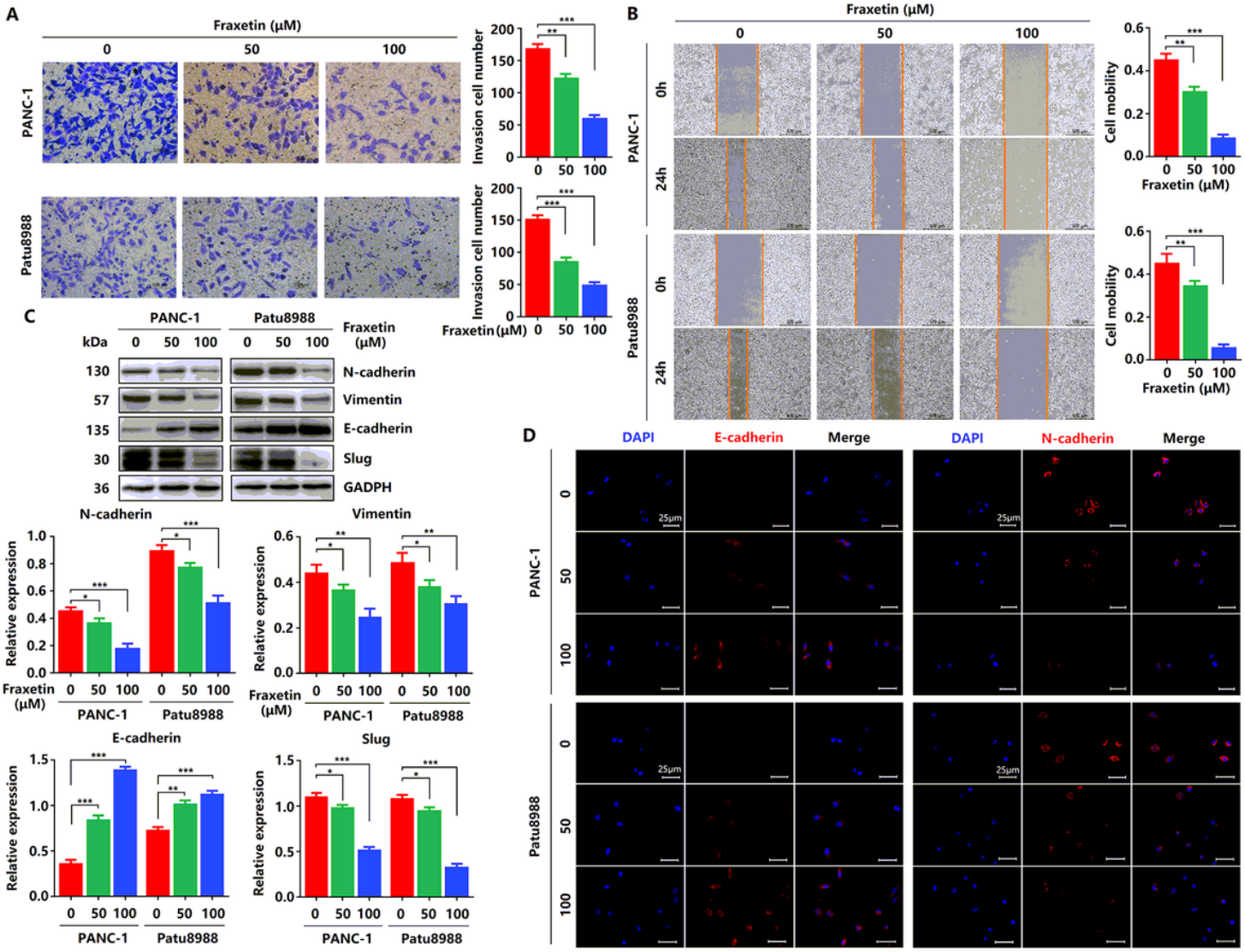

Figure 2

Fraxetin inhibits PCC invasion and migration by regulating the Slug-E-cadherin axis. (A) The effects of fraxetin on the invasion number of PANC-1 and Patu8988 cells were analyzed by transwell chamber assay. (B) The effects of fraxetin on the migrated rate of PANC-1 and Patu8988 cells determined by wound healing assay. (C) Western blot analysis showing the expression of N-cadherin, Vimentin, E-cadherin, and Slug in fraxetin-treated PANC-1 and Patu8988 cells. (D) Immunocytochemical staining of E-cadherin and α-SMA in fraxetin-treated PANC-1 and Patu8988 cells. Bar = 25 μm. Data were presented as the mean ± standard deviation, and were analyzed by One-way ANOVA with Bonferroni's post-hoc test. *P < 0.05, **P < 0.01, ***P < 0.001.

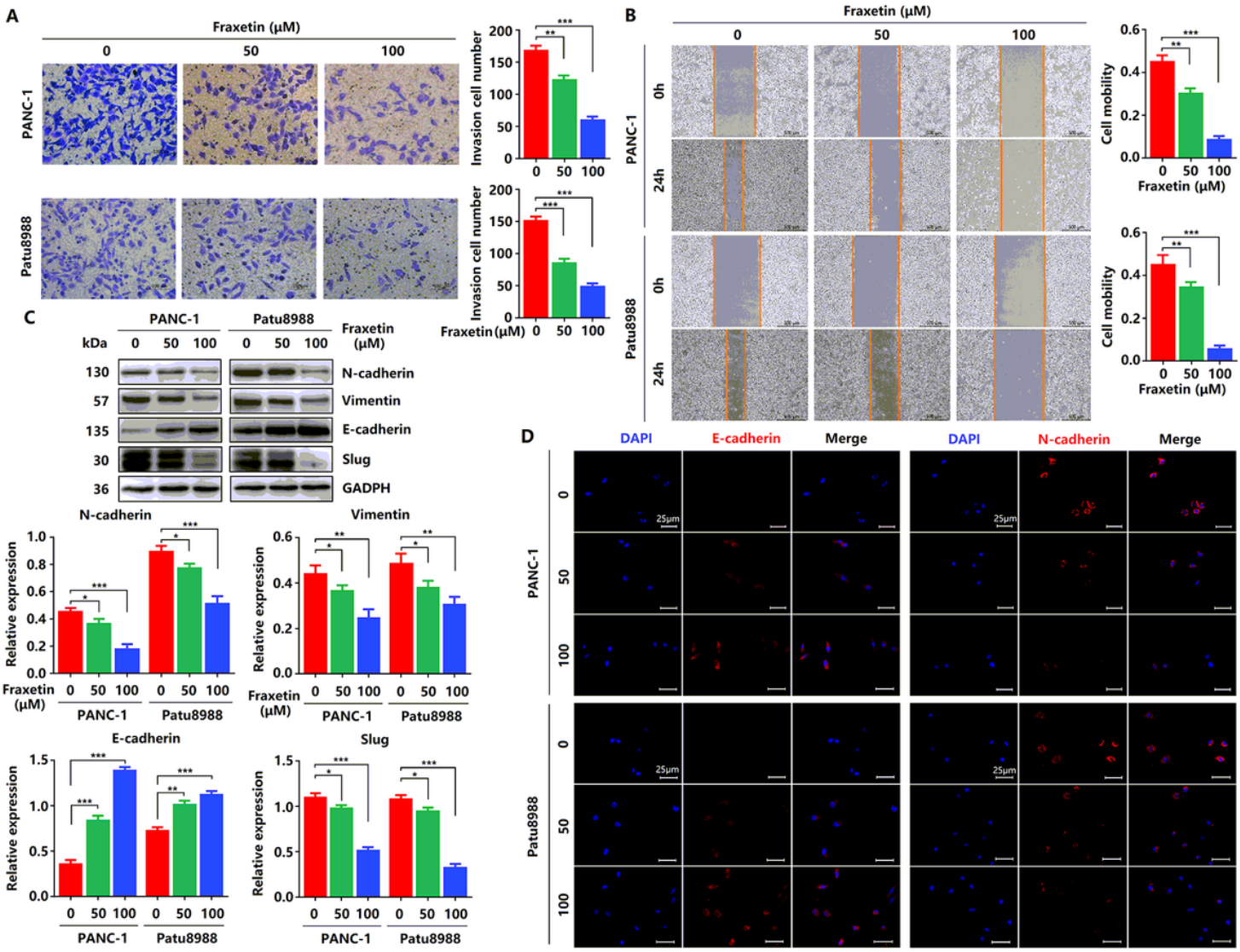

Figure 2

Fraxetin inhibits PCC invasion and migration by regulating the Slug-E-cadherin axis. (A) The effects of fraxetin on the invasion number of PANC-1 and Patu8988 cells were analyzed by transwell chamber assay. (B) The effects of fraxetin on the migrated rate of PANC-1 and Patu8988 cells determined by wound healing assay. (C) Western blot analysis showing the expression of N-cadherin, Vimentin, E-cadherin, and Slug in fraxetin-treated PANC-1 and Patu8988 cells. (D) Immunocytochemical staining of E-cadherin and α-SMA in fraxetin-treated PANC-1 and Patu8988 cells. Bar = 25 μm. Data were presented as the mean ± standard deviation, and were analyzed by One-way ANOVA with Bonferroni's post-hoc test. *P < 0.05, **P < 0.01, ***P < 0.001.

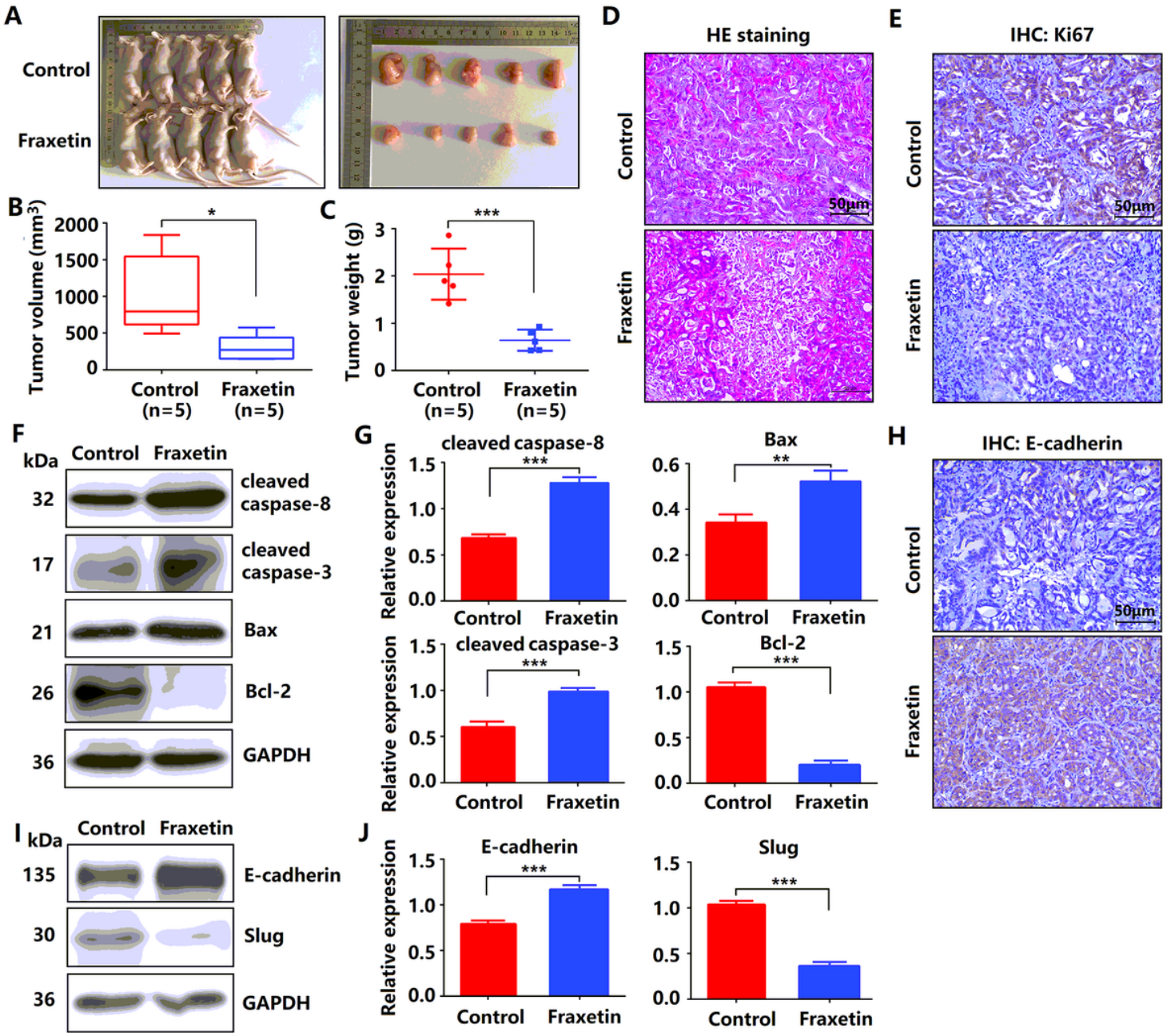

Figure 3

Fraxetin inhibits tumor growth and metastasis of PDA in animal xenograft models. (A) Effects of fraxetin on morphologic changes in experimental groups. (B) Effect of fraxetin on the volume of tumors in animal xenograft models. (C) Effects of fraxetin on tumor weight. (D) HE-staining for PDA pathological results in tissues of the model group. Bar = 50 μm. (E) Immunohistochemical (IHC) staining for Ki67 in fraxetin-treated models. Bar = 50 μm. (F-G) Western blot analysis showing the expression of cleaved caspase-8, cleaved caspase-3, Bax, and Bcl-2 in PANC-1 and Patu8988 cells with or without fraxetin treatment. (H) IHC staining for E-cadherin in fraxetin-treated models. Bar = 50 μm. (I-J) Western blot analysis showing the expression of E-cadherin and Slug in PANC-1 and Patu8988 cells with or without fraxetin treatment. Data were presented as the mean ± standard deviation, and were analyzed by a two-sided Student's t-test. *P < 0.05, **P < 0.01, ***P < 0.001.

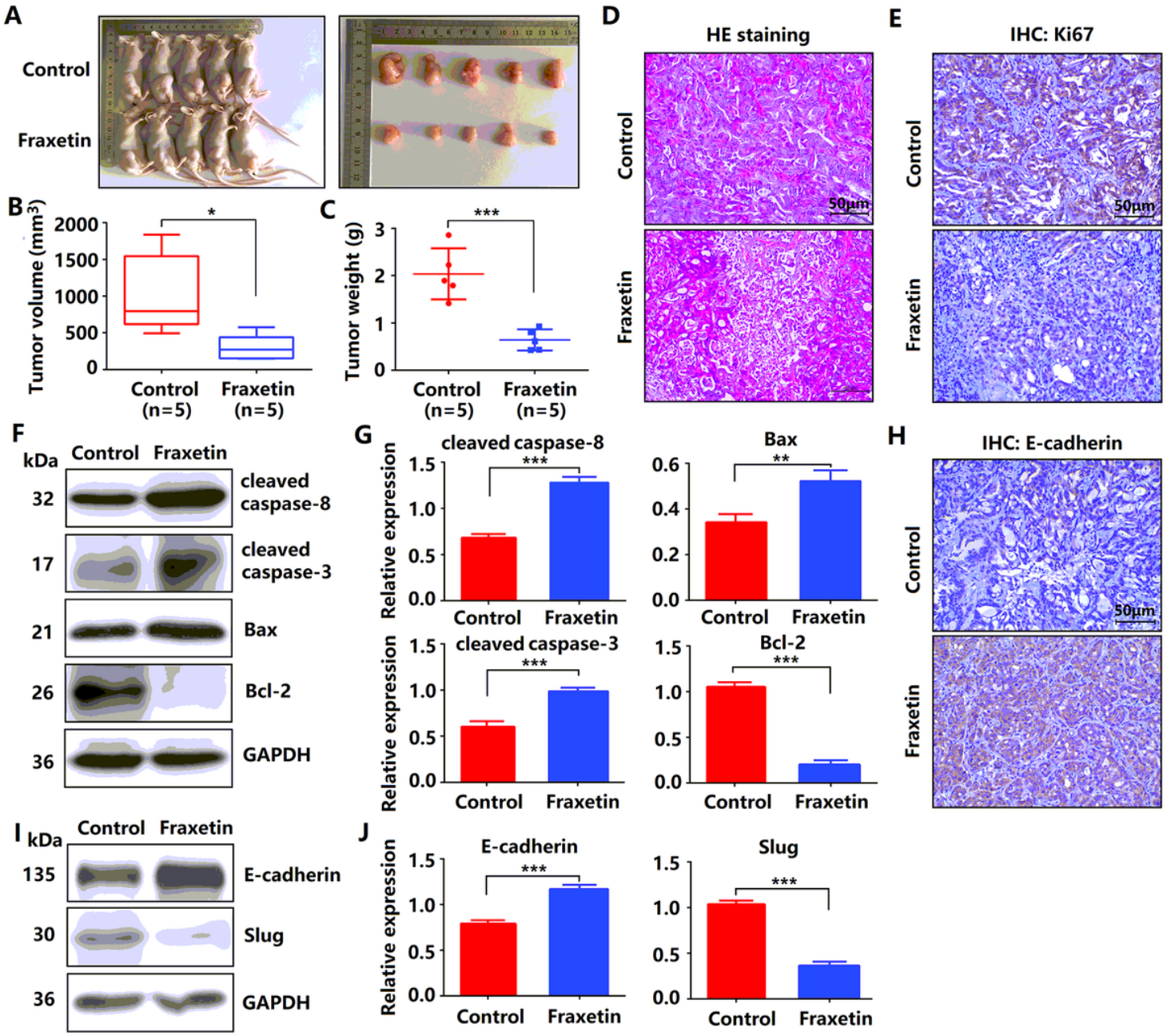

Figure 3

Fraxetin inhibits tumor growth and metastasis of PDA in animal xenograft models. (A) Effects of fraxetin on morphologic changes in experimental groups. (B) Effect of fraxetin on the volume of tumors in animal xenograft models. (C) Effects of fraxetin on tumor weight. (D) HE-staining for PDA pathological results in tissues of the model group. Bar = 50 μm. (E) Immunohistochemical (IHC) staining for Ki67 in fraxetin-treated models. Bar = 50 μm. (F-G) Western blot analysis showing the expression of cleaved caspase-8, cleaved caspase-3, Bax, and Bcl-2 in PANC-1 and Patu8988 cells with or without fraxetin treatment. (H) IHC staining for E-cadherin in fraxetin-treated models. Bar = 50 μm. (I-J) Western blot analysis showing the expression of E-cadherin and Slug in PANC-1 and Patu8988 cells with or without fraxetin treatment. Data were presented as the mean ± standard deviation, and were analyzed by a two-sided Student's t-test. *P < 0.05, **P < 0.01, ***P < 0.001.

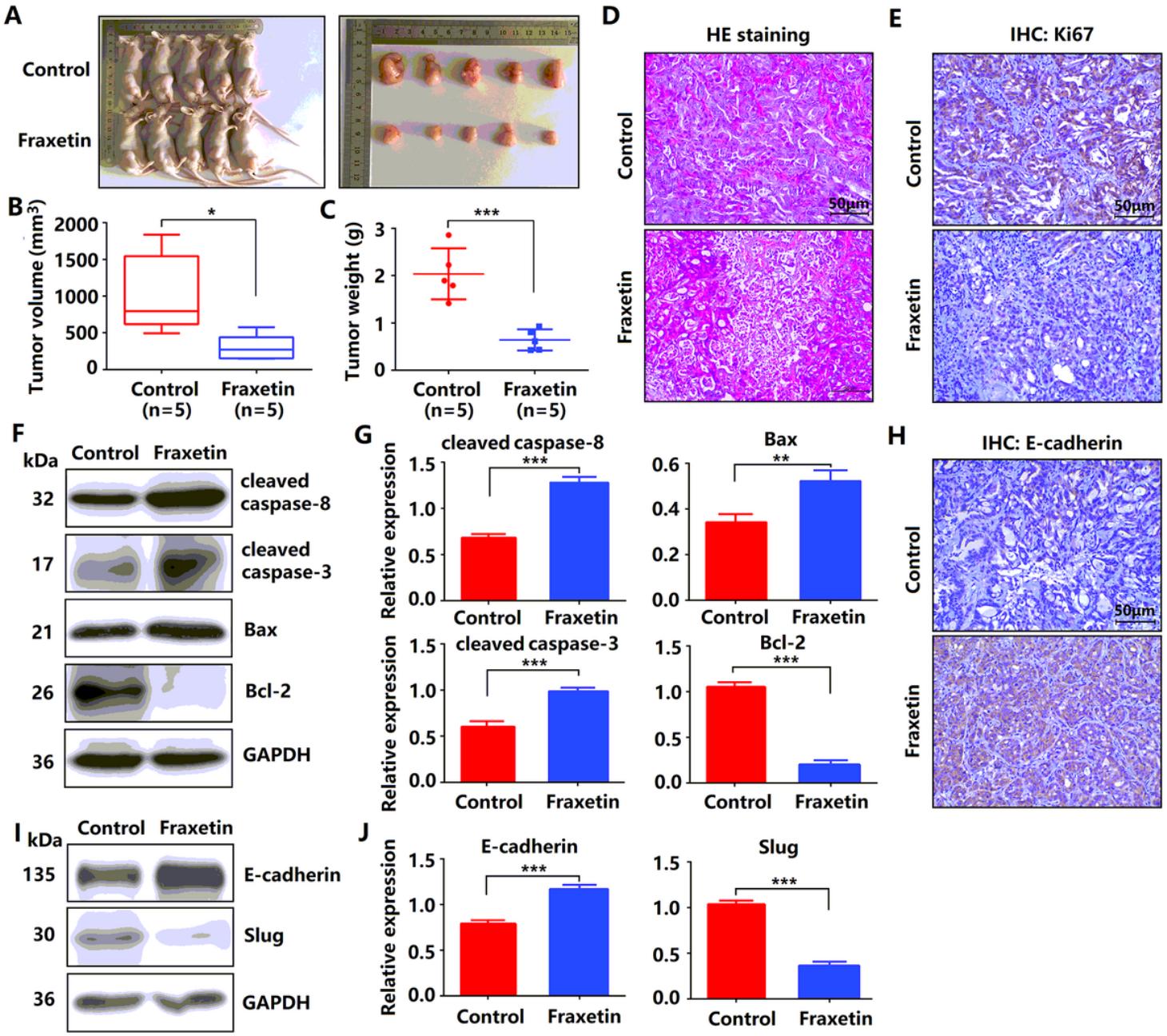

Figure 3

Fraxetin inhibits tumor growth and metastasis of PDA in animal xenograft models. (A) Effects of fraxetin on morphologic changes in experimental groups. (B) Effect of fraxetin on the volume of tumors in animal xenograft models. (C) Effects of fraxetin on tumor weight. (D) HE-staining for PDA pathological results in tissues of the model group. Bar = 50 μm. (E) Immunohistochemical (IHC) staining for Ki67 in fraxetin-treated models. Bar = 50 μm. (F-G) Western blot analysis showing the expression of cleaved caspase-8, cleaved caspase-3, Bax, and Bcl-2 in PANC-1 and Patu8988 cells with or without fraxetin treatment. (H) IHC staining for E-cadherin in fraxetin-treated models. Bar = 50 μm. (I-J) Western blot analysis showing the expression of E-cadherin and Slug in PANC-1 and Patu8988 cells with or without fraxetin treatment. Data were presented as the mean ± standard deviation, and were analyzed by a two-sided Student's t-test. *P < 0.05, **P < 0.01, ***P < 0.001.

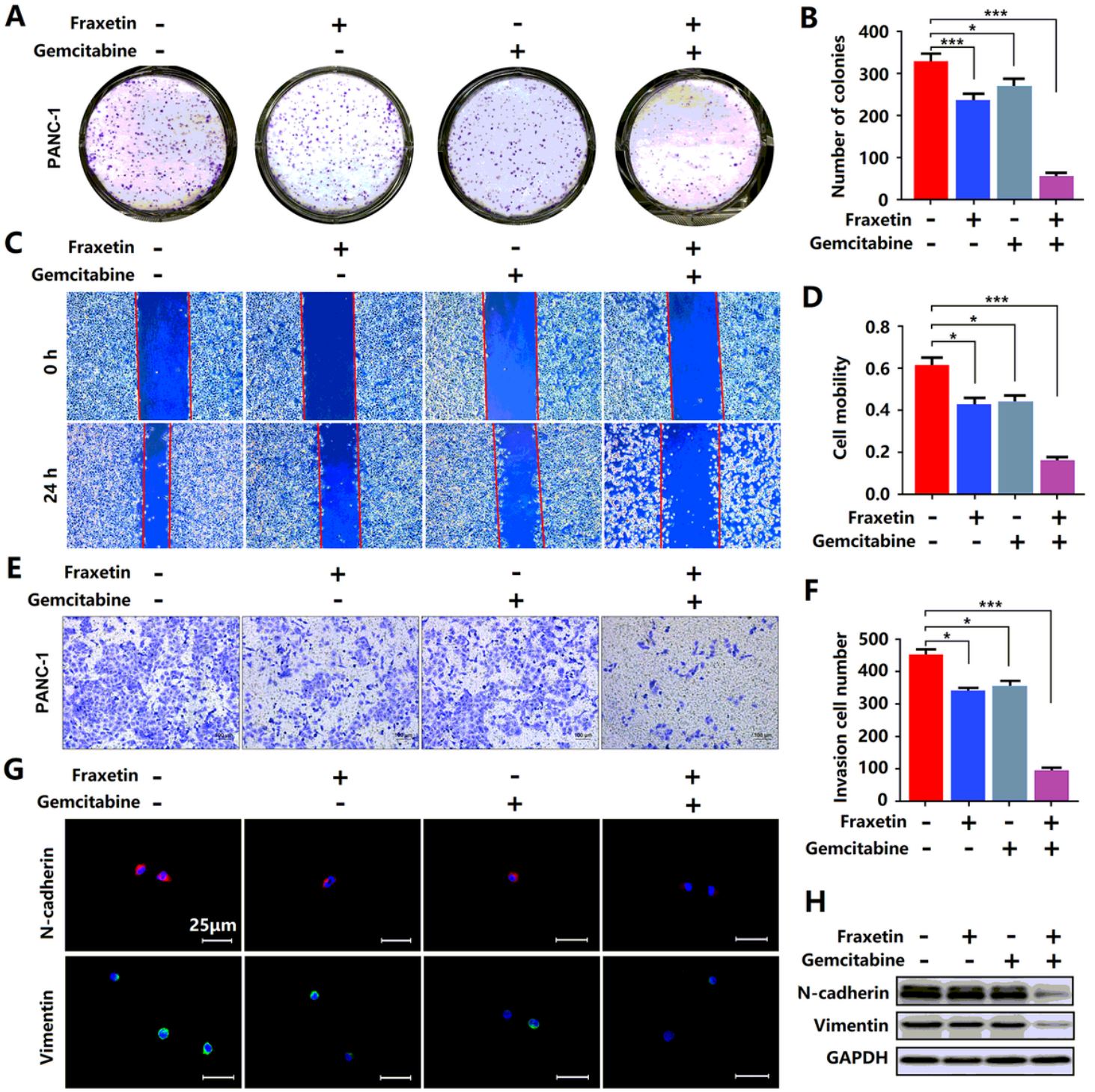

Figure 4

Fraxetin enhanced the sensitivity of PCCs to gemcitabine. (A,B) The effects of fraxetin on the proliferation of gemcitabine-treated PANC-1 cells analyzed by colony formation assay. (C,D) The effects of fraxetin on the migrated rate of gemcitabine-treated PANC-1 cells determined by wound healing assay. (E,F) The effects of fraxetin on the invasion number of gemcitabine-treated PANC-1 cells analyzed by transwell chamber assay. (G) Immunocytochemical staining of N-cadherin and Vimentin in gemcitabine-treated PANC-1 with or without fraxetin treatment. Bar = 50 μm. (H) Western blot analysis showing the expression

of N-cadherin and Vimentin in gemcitabine-treated PANC-1 with or without fraxetin treatment. Data were presented as the mean ± standard deviation, and were analyzed by One-way ANOVA with Bonferroni's post-hoc test and two-sided Student's t-test. *P < 0.05, ***P < 0.001.

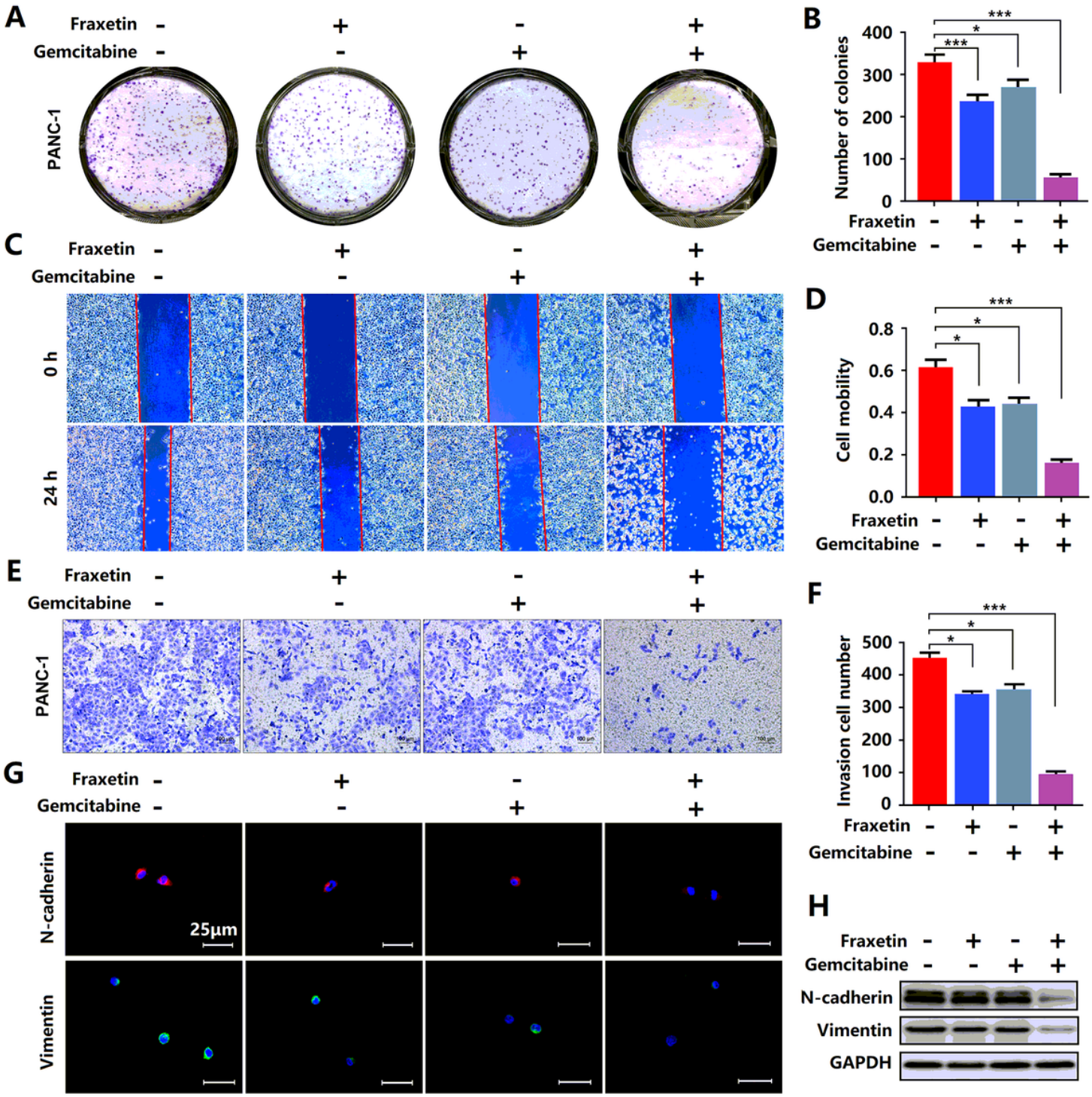

Figure 4

Fraxetin enhanced the sensitivity of PCCs to gemcitabine. (A,B) The effects of fraxetin on the proliferation of gemcitabine-treated PANC-1 cells analyzed by colony formation assay. (C,D) The effects of fraxetin on the migrated rate of gemcitabine-treated PANC-1 cells determined by wound healing assay. (E,F) The

effects of fraxetin on the invasion number of gemcitabine-treated PANC-1 cells analyzed by transwell chamber assay. (G) Immunocytochemical staining of N-cadherin and Vimentin in gemcitabine-treated PANC-1 with or without fraxetin treatment. Bar = 50 μm. (H) Western blot analysis showing the expression of N-cadherin and Vimentin in gemcitabine-treated PANC-1 with or without fraxetin treatment. Data were presented as the mean ± standard deviation, and were analyzed by One-way ANOVA with Bonferroni's post-hoc test and two-sided Student's t-test. *P < 0.05, ***P < 0.001.

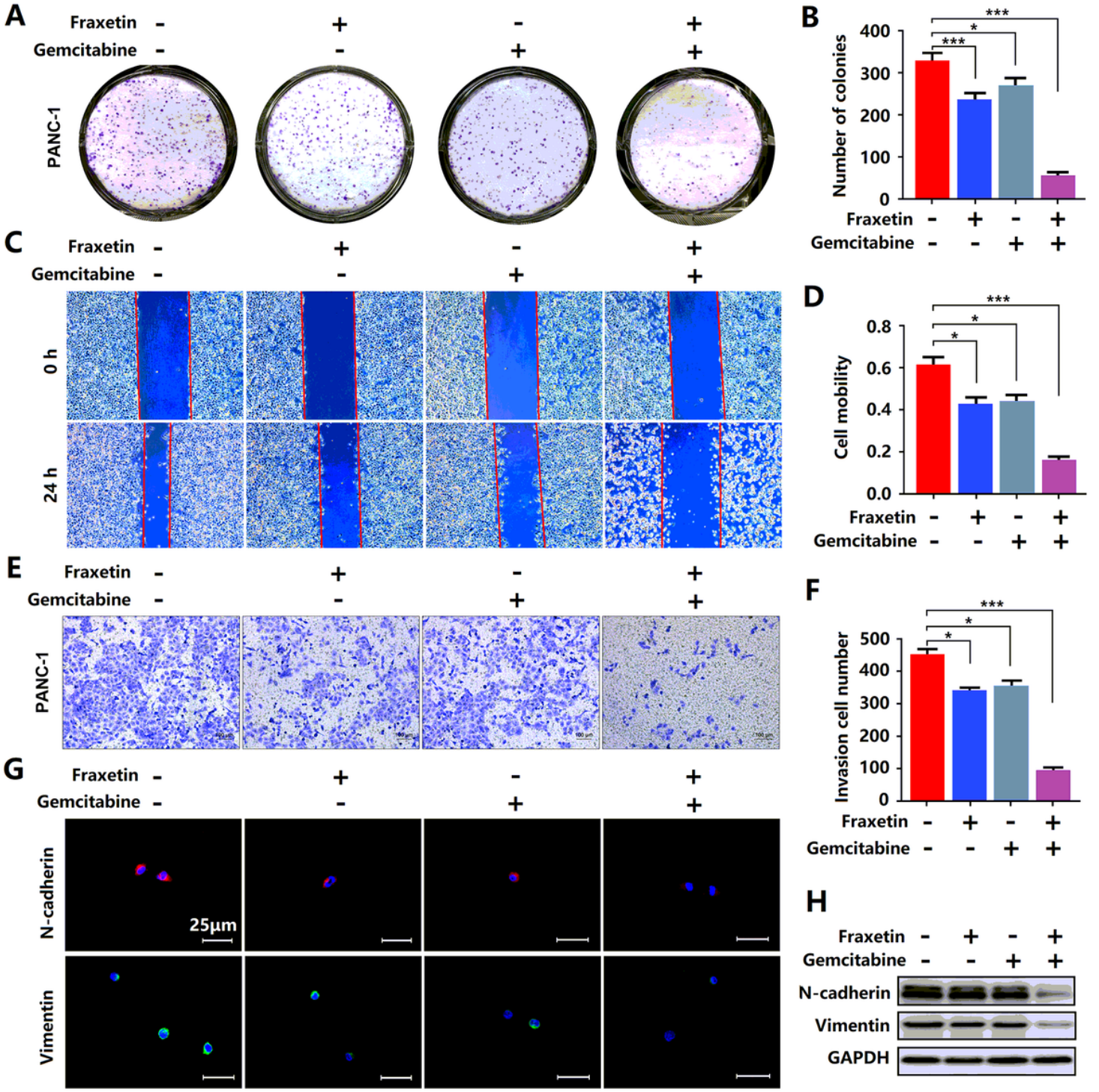

Figure 4

Fraxetin enhanced the sensitivity of PCCs to gemcitabine. (A,B) The effects of fraxetin on the proliferation of gemcitabine-treated PANC-1 cells analyzed by colony formation assay. (C,D) The effects of fraxetin on the migrated rate of gemcitabine-treated PANC-1 cells determined by wound healing assay. (E,F) The effects of fraxetin on the invasion number of gemcitabine-treated PANC-1 cells analyzed by transwell chamber assay. (G) Immunocytochemical staining of N-cadherin and Vimentin in gemcitabine-treated PANC-1 with or without fraxetin treatment. Bar = 50 μm. (H) Western blot analysis showing the expression of N-cadherin and Vimentin in gemcitabine-treated PANC-1 with or without fraxetin treatment. Data were presented as the mean ± standard deviation, and were analyzed by One-way ANOVA with Bonferroni's post-hoc test and two-sided Student's t-test. *P < 0.05, ***P < 0.001.

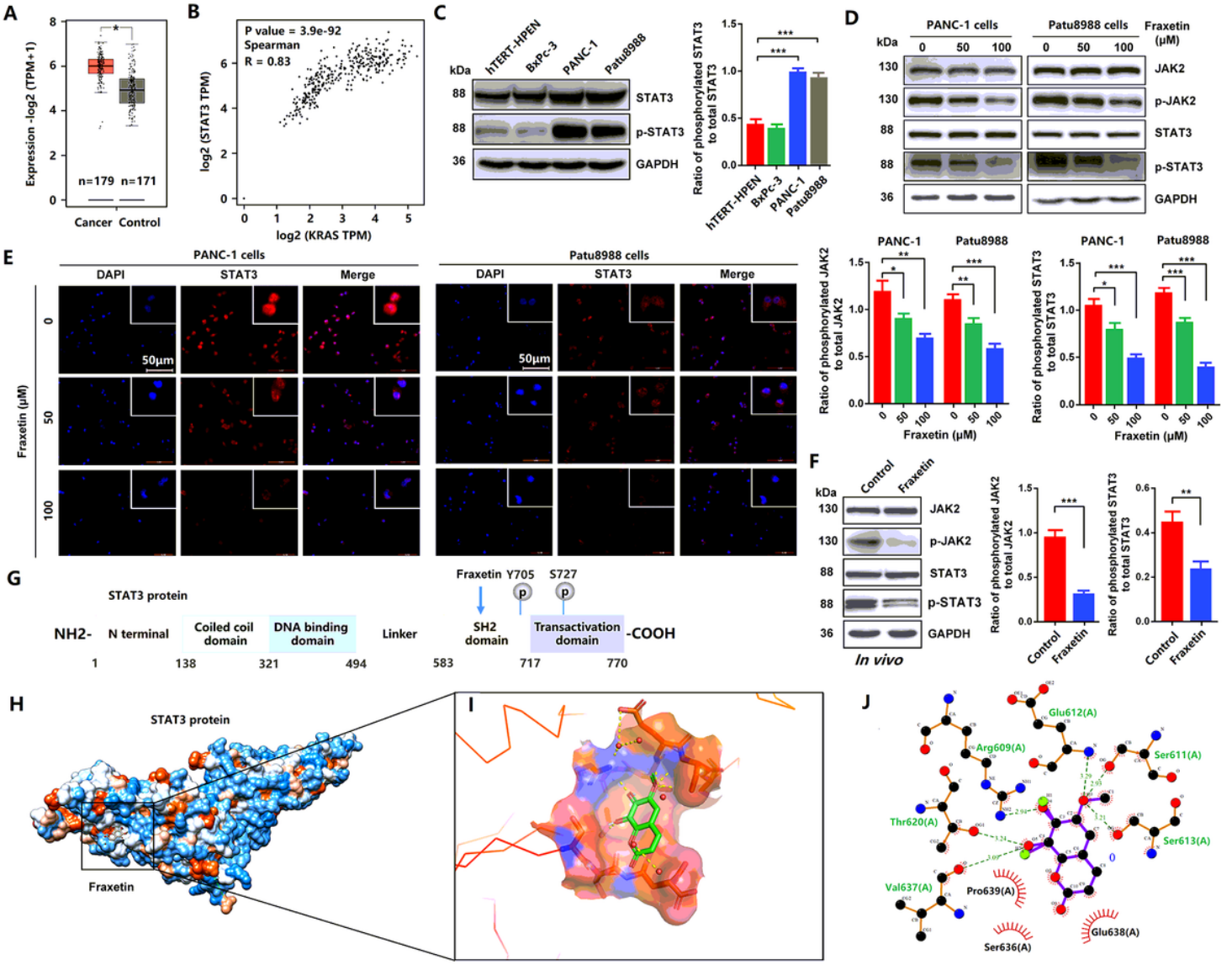

Figure 5

Fraxetin induced STAT3 inactivation by occupying its SH2 domain in vitro and in vivo. (A) The expression of STAT3 in PDA tissues and adjacent normal tissues in the GEPIA 2 database was analyzed. (B) The correlation between STAT3 expression and KRAS activity in the GEPIA 2 database was evaluated. (C) The expression and phosphorylation of STAT3 in a normal pancreatic ductal cell (hTERT-HPENKRAS(-)) and

PCCs (PANC-1KRAS G12D, Patu8988KRAS G12V and BxPc-3KRAS(-)) (D) Western blot analysis showing the expression and phosphorylation of JAK2 and STAT3 in PANC-1 and Patu8988 cells with or without fraxetin treatment. (E) Immunocytochemical staining of STAT3 in PANC-1 and Patu8988 cells with or without fraxetin treatment. Bar = 50 μm. (F) Western blot analysis showing the expression and phosphorylation of JAK2 and STAT3 in fraxetin-treated animal xenograft models. The overview of Fraxetin binding in the STAT3 SH2 domain by using UCSF chimera. (G) Sequence analysis indicates that the STAT3 protein harbor conserved motifs, such as the DNA binding region and SH2 domain. (H) The overview of Fraxetin binding in the STAT3 SH2 domain by using UCSF chimera. (I) 3D representation of fraxetin binding sites in the STAT3 SH2 domain (yellow dotted line means hydrogen bond) by using PyMol. (J) Detailed 2D representation of fraxetin binding sites in STAT3 SH2 domain residues interactions generated by LigPlot plus. Data were presented as the mean ± standard deviation, and were analyzed by One-way ANOVA with Bonferroni's post-hoc test and two-sided Student's t-test. *P < 0.05, **P < 0.01, ***P < 0.001.

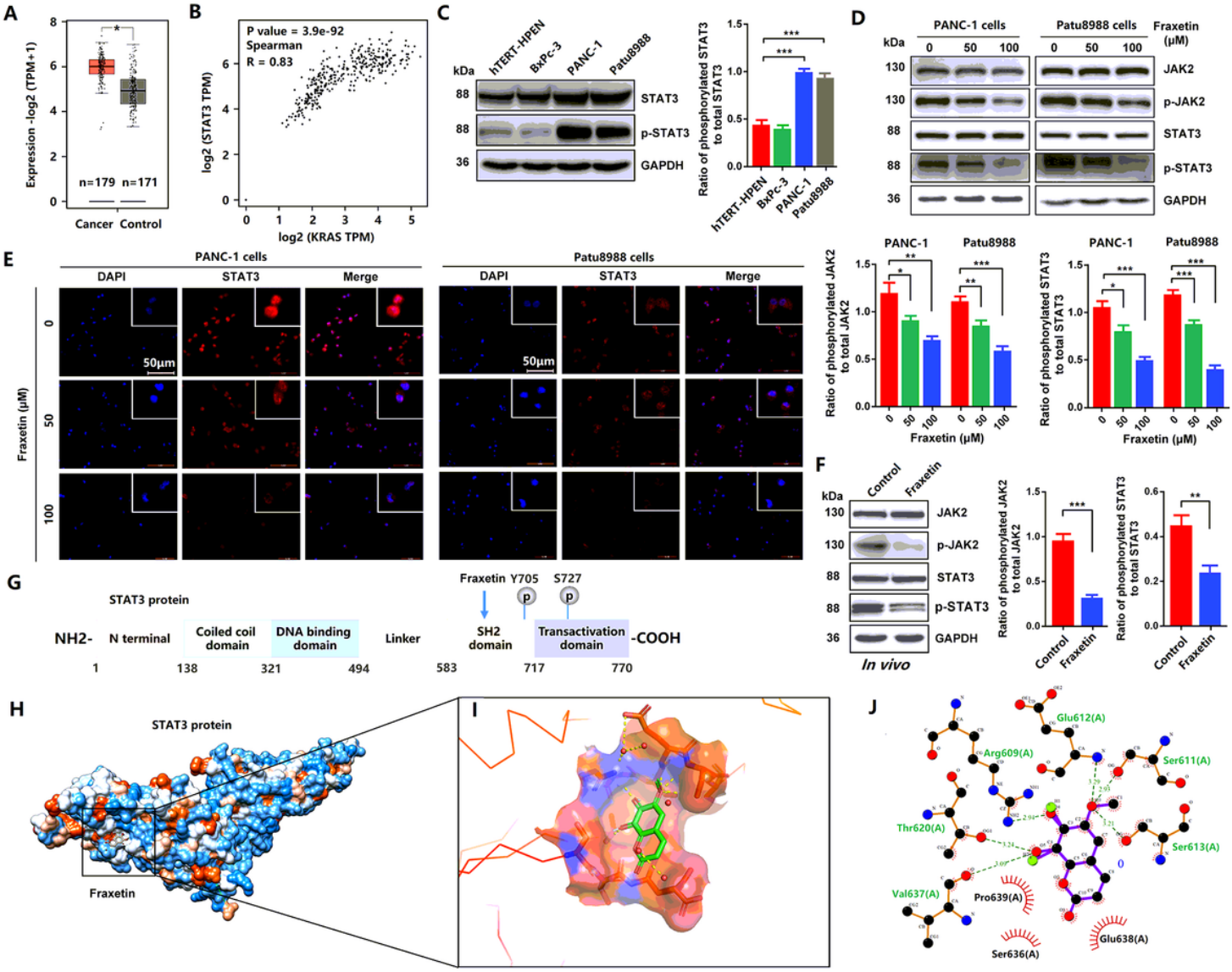

Figure 5

Fraxetin induced STAT3 inactivation by occupying its SH2 domain in vitro and in vivo. (A) The expression of STAT3 in PDA tissues and adjacent normal tissues in the GEPIA 2 database was analyzed. (B) The correlation between STAT3 expression and KRAS activity in the GEPIA 2 database was evaluated. (C) The expression and phosphorylation of STAT3 in a normal pancreatic ductal cell (hTERT-HPENKRAS(-)) and PCCs (PANC-1KRAS G12D, Patu8988KRAS G12V and BxPc-3KRAS(-)) (D) Western blot analysis showing the expression and phosphorylation of JAK2 and STAT3 in PANC-1 and Patu8988 cells with or without fraxetin treatment. (E) Immunocytochemical staining of STAT3 in PANC-1 and Patu8988 cells with or without fraxetin treatment. Bar = 50 μm. (F) Western blot analysis showing the expression and phosphorylation of JAK2 and STAT3 in fraxetin-treated animal xenograft models. The overview of Fraxetin binding in the STAT3 SH2 domain by using UCSF chimera. (G) Sequence analysis indicates that the STAT3 protein harbor conserved motifs, such as the DNA binding region and SH2 domain. (H) The overview of Fraxetin binding in the STAT3 SH2 domain by using UCSF chimera. (I) 3D representation of fraxetin binding sites in the STAT3 SH2 domain (yellow dotted line means hydrogen bond) by using PyMol. (J) Detailed 2D representation of fraxetin binding sites in STAT3 SH2 domain residues interactions generated by LigPlot plus. Data were presented as the mean ± standard deviation, and were analyzed by One-way ANOVA with Bonferroni's post-hoc test and two-sided Student’s t-test. *P < 0.05, **P < 0.01, ***P < 0.001.

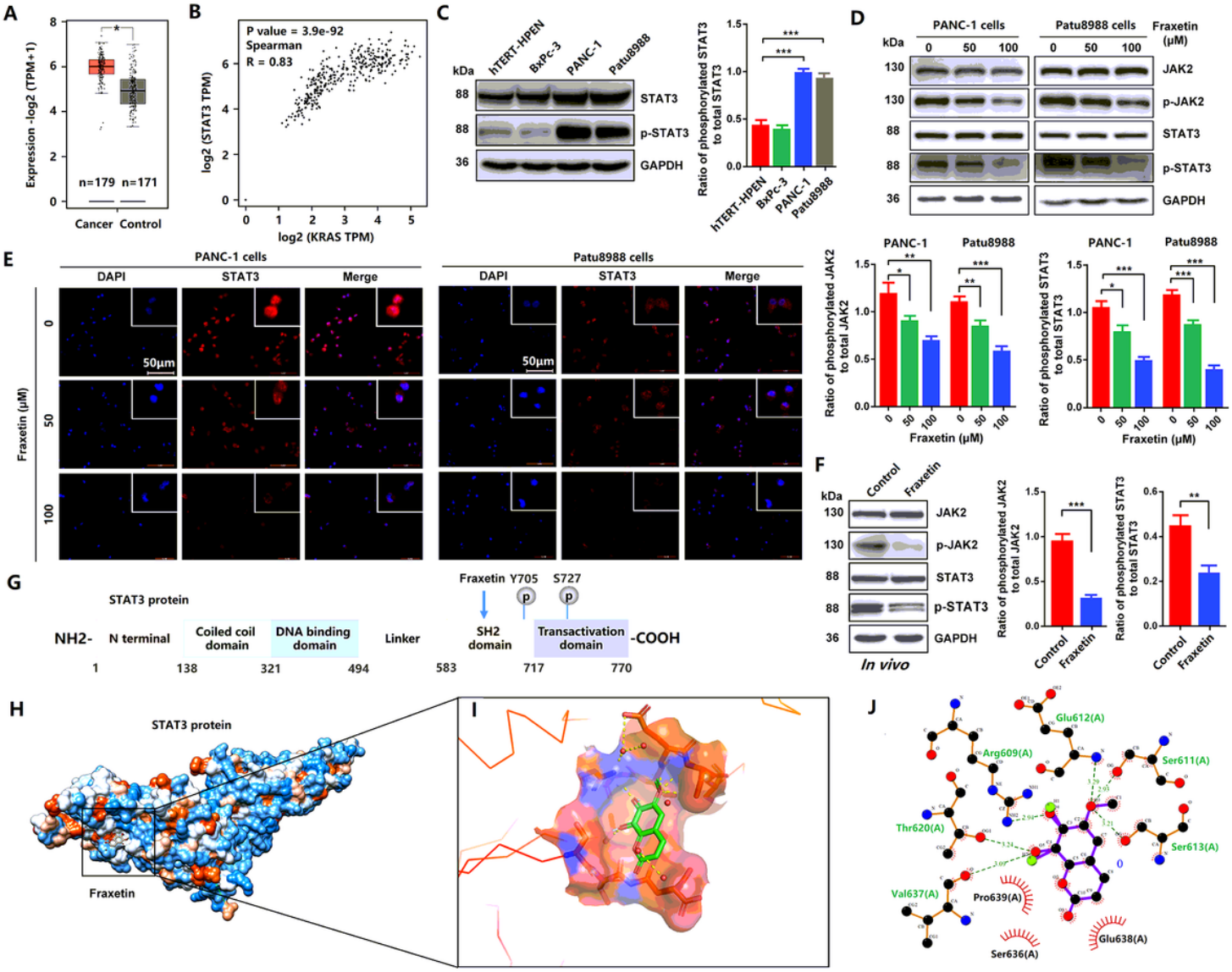

Figure 5

Fraxetin induced STAT3 inactivation by occupying its SH2 domain in vitro and in vivo. (A) The expression of STAT3 in PDA tissues and adjacent normal tissues in the GEPIA 2 database was analyzed. (B) The correlation between STAT3 expression and KRAS activity in the GEPIA 2 database was evaluated. (C) The expression and phosphorylation of STAT3 in a normal pancreatic ductal cell (hTERT-HPENKRAS(-)) and PCCs (PANC-1KRAS G12D, Patu8988KRAS G12V and BxPc-3KRAS(-)) (D) Western blot analysis showing the expression and phosphorylation of JAK2 and STAT3 in PANC-1 and Patu8988 cells with or without fraxetin treatment. (E) Immunocytochemical staining of STAT3 in PANC-1 and Patu8988 cells with or without fraxetin treatment. Bar = 50 μm. (F) Western blot analysis showing the expression and phosphorylation of JAK2 and STAT3 in fraxetin-treated animal xenograft models. The overview of Fraxetin binding in the STAT3 SH2 domain by using UCSF chimera. (G) Sequence analysis indicates that the STAT3 protein harbor conserved motifs, such as the DNA binding region and SH2 domain. (H) The overview of Fraxetin binding in the STAT3 SH2 domain by using UCSF chimera. (I) 3D representation of fraxetin binding sites in the STAT3 SH2 domain (yellow dotted line means hydrogen bond) by using

PyMol. (J) Detailed 2D representation of fraxetin binding sites in STAT3 SH2 domain residues interactions generated by LigPlot plus. Data were presented as the mean ± standard deviation, and were analyzed by One-way ANOVA with Bonferroni's post-hoc test and two-sided Student's t-test. *P < 0.05, **P < 0.01, ***P < 0.001.

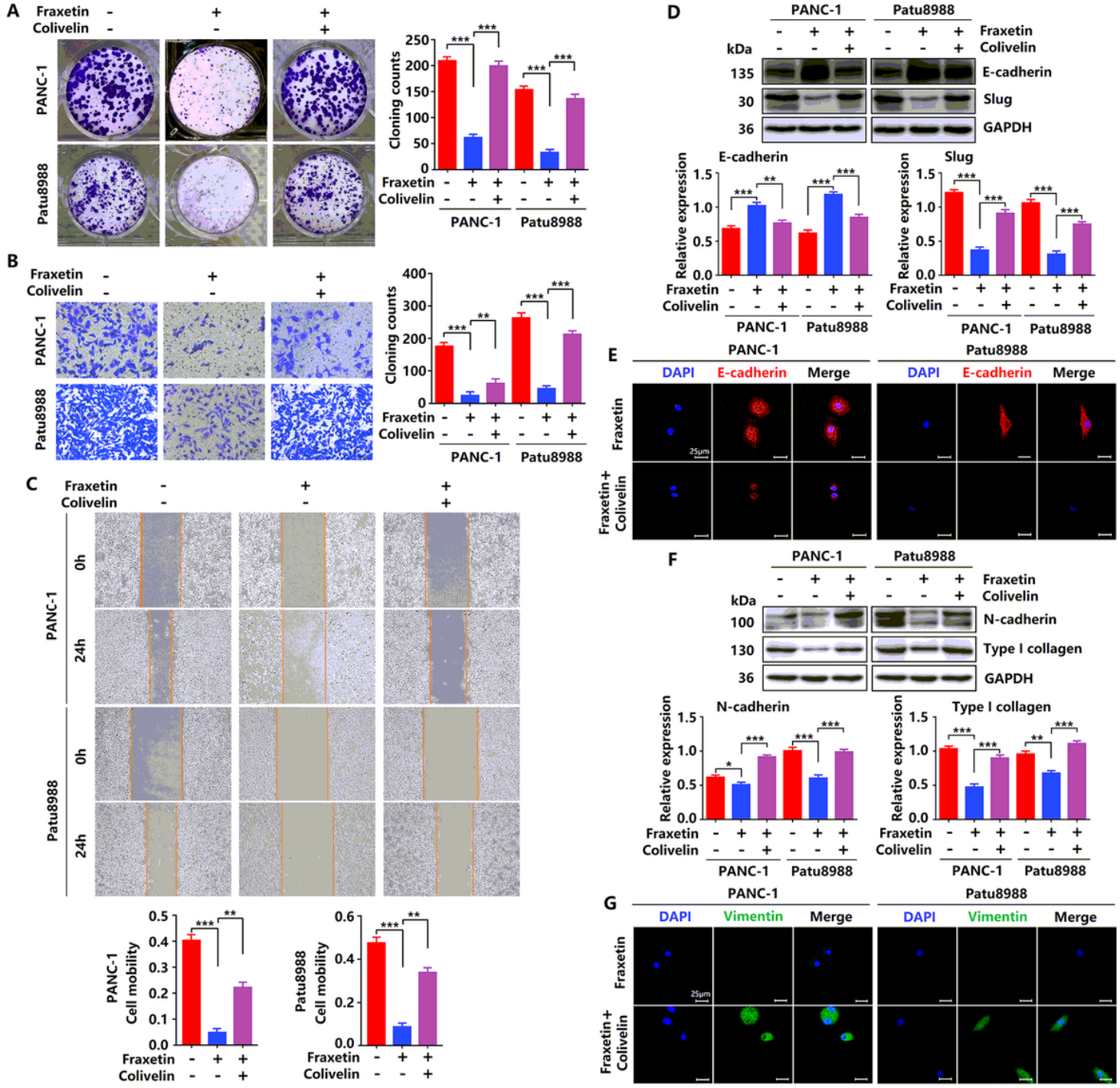

Figure 6

Reactivation of STAT3 reverses the anti-tumor effects of fraxetin. (A) The proliferation of fraxetin-treated PANC-1 and Patu8988 cells with or without colivelin treatment was analyzed by colony formation assay. (B) The invasion ability of fraxetin-treated PANC-1 and Patu8988 cells with or without colivelin treatment

was analyzed by transwell chamber assay. (C) The migration ability of fraxetin-treated PANC-1 and Patu8988 cells with or without colivelin treatment determined by wound healing assay. (D) Western blot analysis showing the expression of E-cadherin and Slug in fraxetin-treated PANC-1 and Patu8988 cells with or without colivelin treatment. (E) Immunocytochemical staining of E-cadherin in fraxetin-treated PANC-1 and Patu8988 cells with or without colivelin treatment. Bar = 25 μm. (F) Western blot analysis showing the expression of N-cadherin and Type I collagen in fraxetin-treated PANC-1 and Patu8988 cells with or without colivelin treatment. (G) Immunocytochemical staining of vimentin in fraxetin-treated PANC-1 and Patu8988 cells with or without colivelin treatment. Bar = 25 μm. Data were presented as the mean ± standard deviation, and were analyzed by One-way ANOVA with Bonferroni's post-hoc test and two-sided Student's t-test.. *P < 0.05, **P < 0.01, ***P < 0.001.

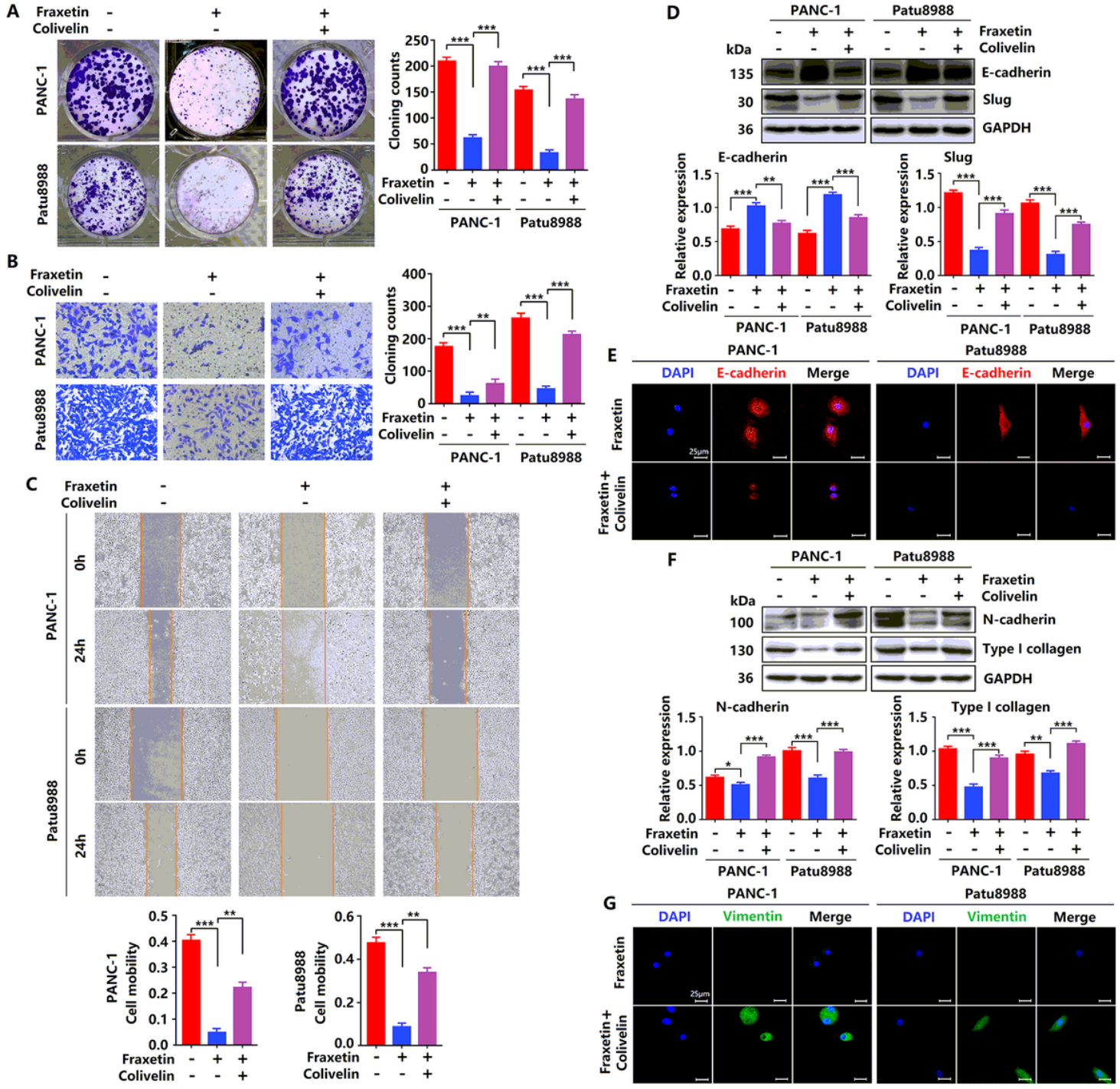

Figure 6

Reactivation of STAT3 reverses the anti-tumor effects of fraxetin. (A) The proliferation of fraxetin-treated PANC-1 and Patu8988 cells with or without colivelin treatment was analyzed by colony formation assay. (B) The invasion ability of fraxetin-treated PANC-1 and Patu8988 cells with or without colivelin treatment was analyzed by transwell chamber assay. (C) The migration ability of fraxetin-treated PANC-1 and Patu8988 cells with or without colivelin treatment determined by wound healing assay. (D) Western blot analysis showing the expression of E-cadherin and Slug in fraxetin-treated PANC-1 and Patu8988 cells with or without colivelin treatment. (E) Immunocytochemical staining of E-cadherin in fraxetin-treated PANC-1 and Patu8988 cells with or without colivelin treatment. Bar = 25 μm. (F) Western blot analysis showing the expression of N-cadherin and Type I collagen in fraxetin-treated PANC-1 and Patu8988 cells with or without colivelin treatment. (G) Immunocytochemical staining of vimentin in fraxetin-treated PANC-1 and Patu8988 cells with or without colivelin treatment. Bar = 25 μm. Data were presented as the mean ± standard deviation, and were analyzed by One-way ANOVA with Bonferroni's post-hoc test and two-sided Student’s t-test.. *P < 0.05, **P < 0.01, ***P < 0.001.

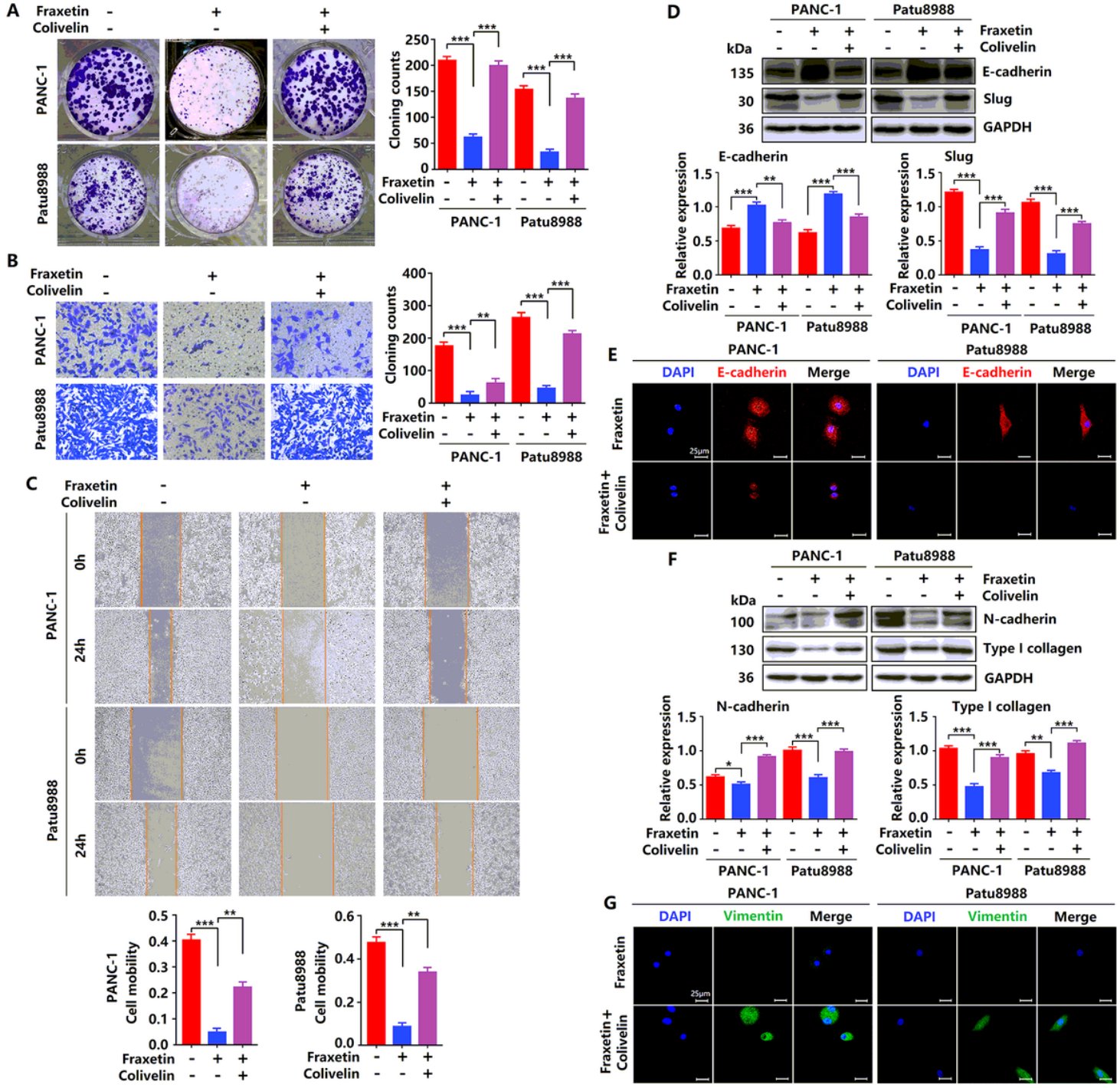

Figure 6

Reactivation of STAT3 reverses the anti-tumor effects of fraxetin. (A) The proliferation of fraxetin-treated PANC-1 and Patu8988 cells with or without colivelin treatment was analyzed by colony formation assay. (B) The invasion ability of fraxetin-treated PANC-1 and Patu8988 cells with or without colivelin treatment was analyzed by transwell chamber assay. (C) The migration ability of fraxetin-treated PANC-1 and Patu8988 cells with or without colivelin treatment determined by wound healing assay. (D) Western blot analysis showing the expression of E-cadherin and Slug in fraxetin-treated PANC-1 and Patu8988 cells with or without colivelin treatment. (E) Immunocytochemical staining of E-cadherin in fraxetin-treated

PANC-1 and Patu8988 cells with or without colivelin treatment. Bar = 25 μm. (F) Western blot analysis showing the expression of N-cadherin and Type I collagen in fraxetin-treated PANC-1 and Patu8988 cells with or without colivelin treatment. (G) Immunocytochemical staining of vimentin in fraxetin-treated PANC-1 and Patu8988 cells with or without colivelin treatment. Bar = 25 μm. Data were presented as the mean ± standard deviation, and were analyzed by One-way ANOVA with Bonferroni's post-hoc test and two-sided Student's t-test.. *P < 0.05, **P < 0.01, ***P < 0.001.

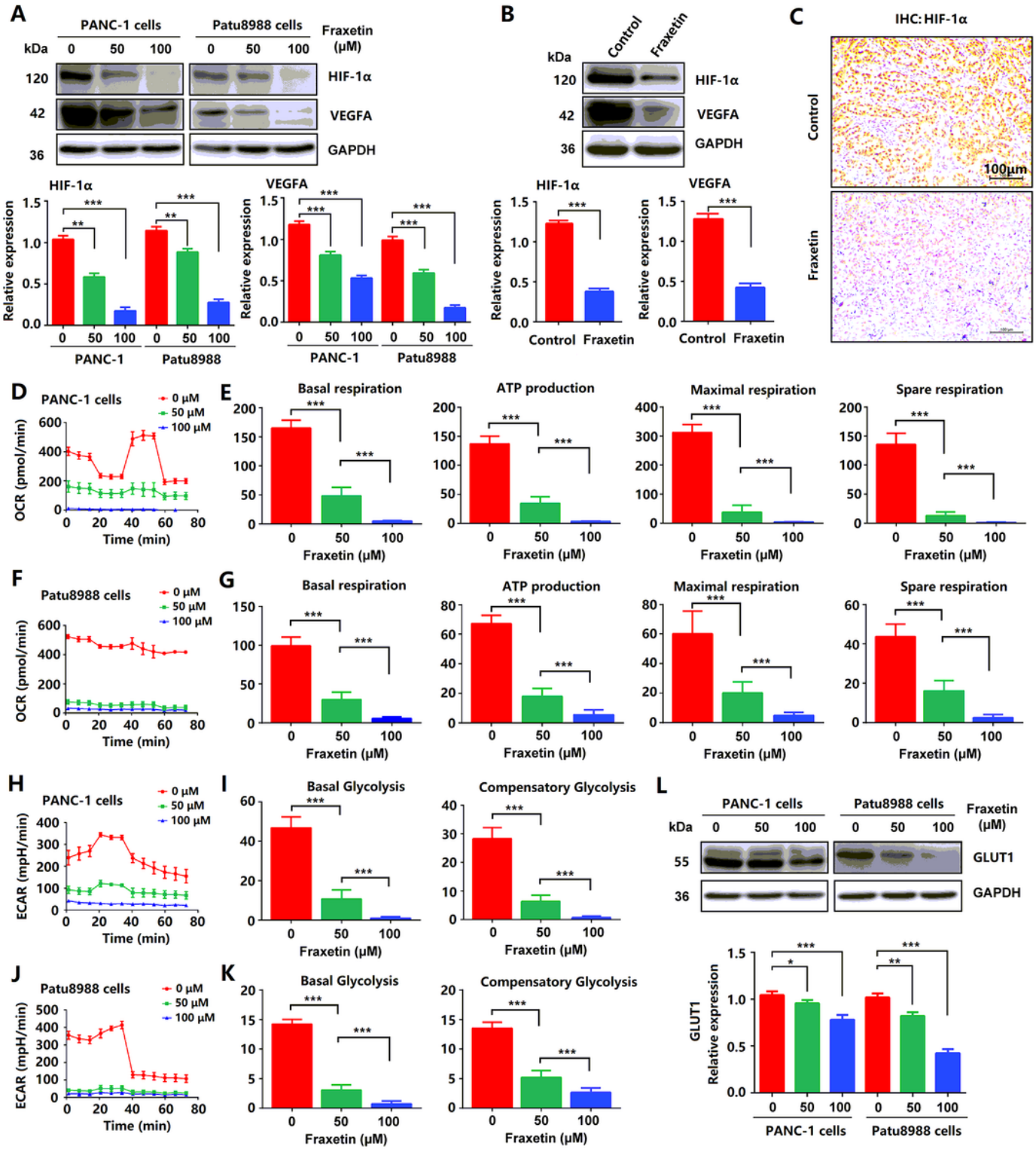

Figure 7

Fraxetin inhibited angiogenesis, glucose metabolism and EMT in PCCs. (A) Western blot analysis showing the expression of HIF-1α and VEGFA in fraxetin-treated PANC-1 and Patu8988 cells. (B) Western blot analysis showing the expression of HIF-1α and VEGFA in fraxetin-treated animal xenograft models. (C) IHC staining for HIF-1α in fraxetin-treated models. Bar = 100 μm. (D-G) Glucose metabolism assay showing downregulated levels of oxygen consumption rate (OCR), basal respiration, spare respiration, maximal respiration, and ATP production in fraxetin-treated PANC-1 and Patu8988 cells. (H-K) Glucose metabolism assay showing reduced levels of extracellular acidification rate (ECAR), basal glycolysis and compensatory glycolysis in fraxetin-treated PANC-1 and Patu8988 cells. (L) Western blot analysis showing GLUT1 expression in fraxetin-treated PANC-1 and Patu8988 cells. Data were presented as the mean ± standard deviation, and were analyzed by One-way ANOVA with Bonferroni's post-hoc test and two-sided Student’s t-test.. *P < 0.05; **P < 0.01, ***P < 0.001.

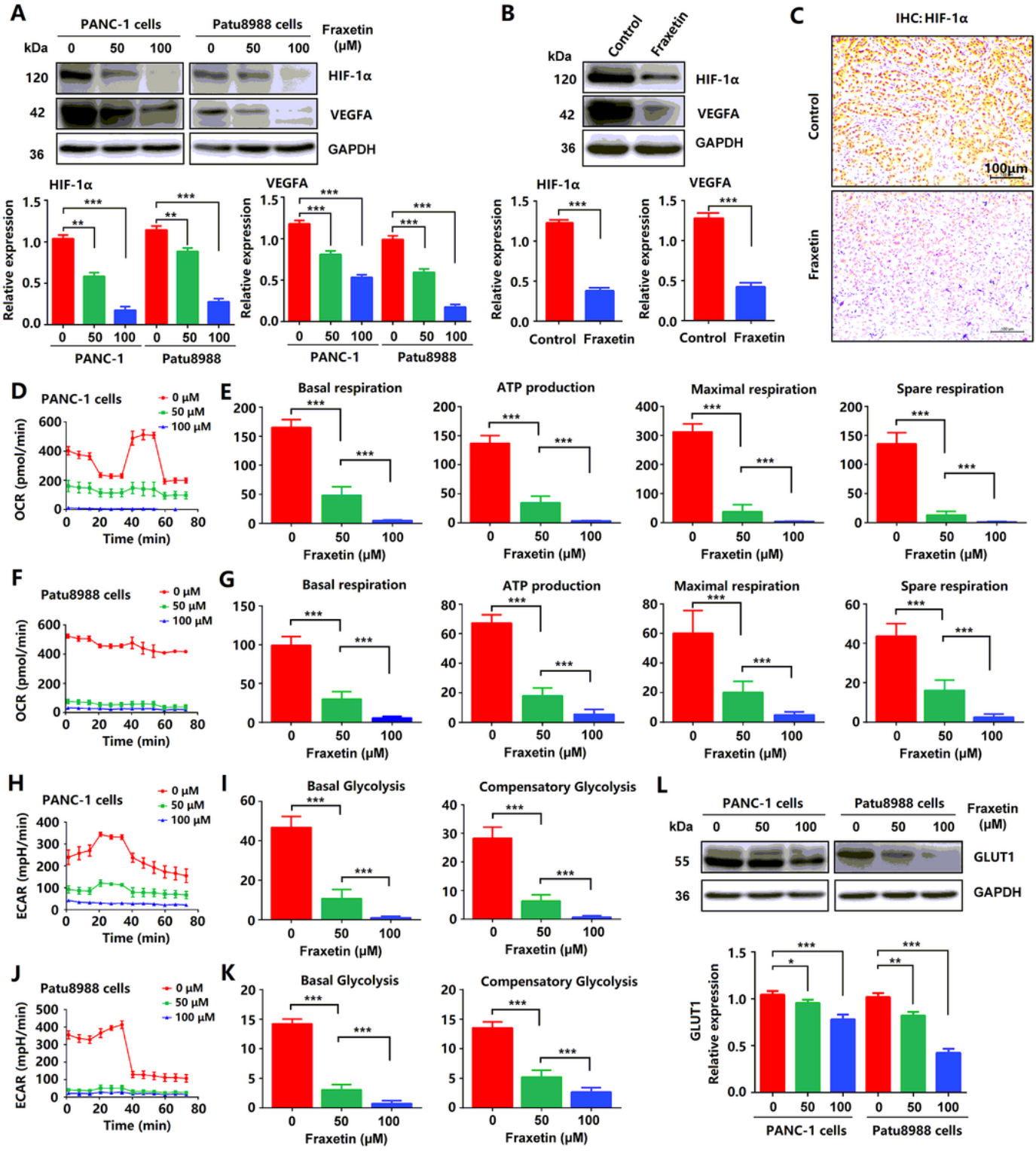

Figure 7

Fraxetin inhibited angiogenesis, glucose metabolism and EMT in PCCs. (A) Western blot analysis showing the expression of HIF-1α and VEGFA in fraxetin-treated PANC-1 and Patu8988 cells. (B) Western blot analysis showing the expression of HIF-1α and VEGFA in fraxetin-treated animal xenograft models. (C) IHC staining for HIF-1α in fraxetin-treated models. Bar = 100 μm. (D-G) Glucose metabolism assay showing downregulated levels of oxygen consumption rate (OCR), basal respiration, spare respiration,

maximal respiration, and ATP production in fraxetin-treated PANC-1 and Patu8988 cells. (H-K) Glucose metabolism assay showing reduced levels of extracellular acidification rate (ECAR), basal glycolysis and compensatory glycolysis in fraxetin-treated PANC-1 and Patu8988 cells. (L) Western blot analysis showing GLUT1 expression in fraxetin-treated PANC-1 and Patu8988 cells. Data were presented as the mean ± standard deviation, and were analyzed by One-way ANOVA with Bonferroni's post-hoc test and two-sided Student's t-test.. *P < 0.05; **P < 0.01, ***P < 0.001.

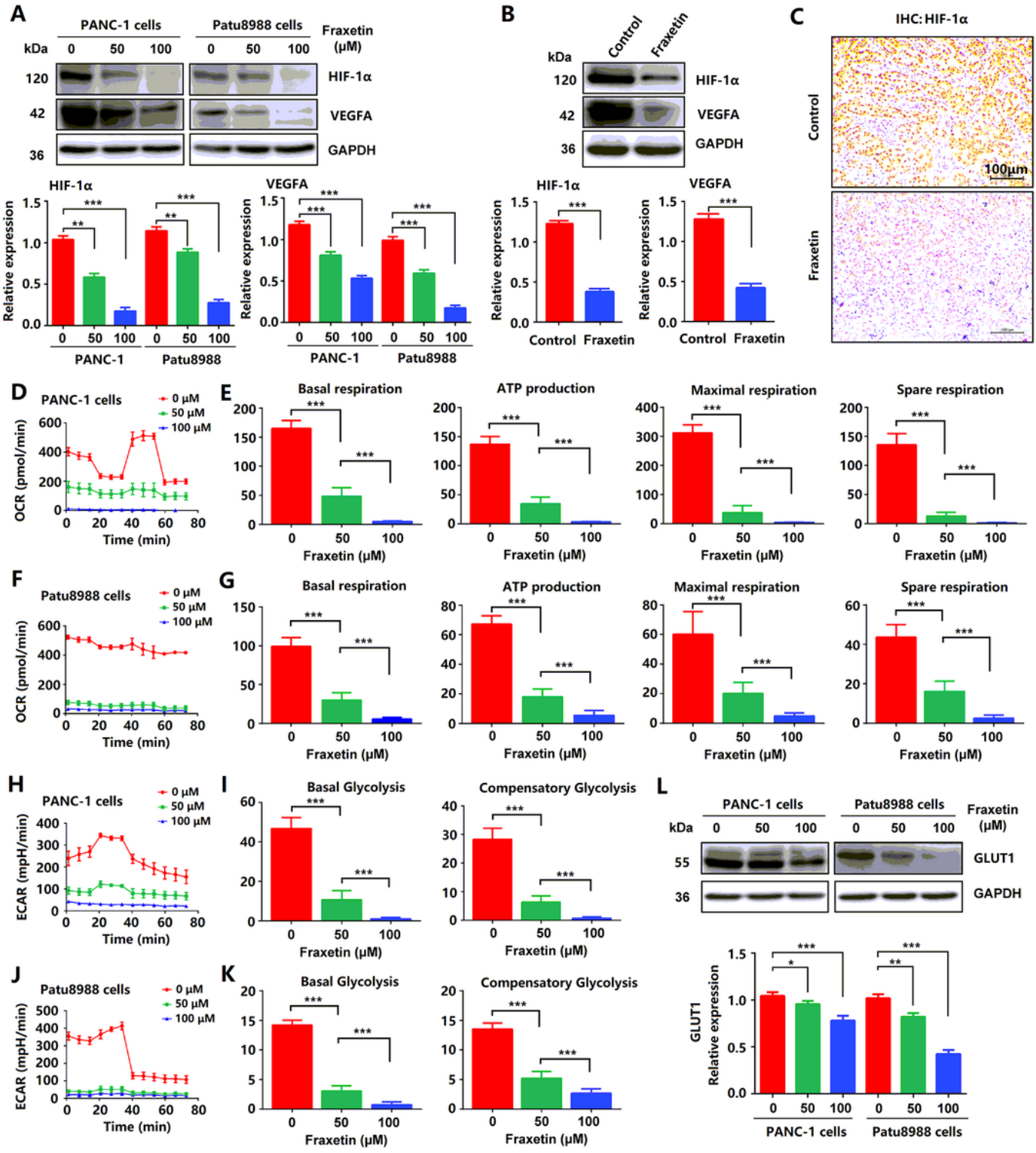

Figure 7

Fraxetin inhibited angiogenesis, glucose metabolism and EMT in PCCs. (A) Western blot analysis showing the expression of HIF-1α and VEGFA in fraxetin-treated PANC-1 and Patu8988 cells. (B) Western blot analysis showing the expression of HIF-1α and VEGFA in fraxetin-treated animal xenograft models. (C) IHC staining for HIF-1α in fraxetin-treated models. Bar = 100 μm. (D-G) Glucose metabolism assay showing downregulated levels of oxygen consumption rate (OCR), basal respiration, spare respiration, maximal respiration, and ATP production in fraxetin-treated PANC-1 and Patu8988 cells. (H-K) Glucose metabolism assay showing reduced levels of extracellular acidification rate (ECAR), basal glycolysis and compensatory glycolysis in fraxetin-treated PANC-1 and Patu8988 cells. (L) Western blot analysis showing GLUT1 expression in fraxetin-treated PANC-1 and Patu8988 cells. Data were presented as the mean ± standard deviation, and were analyzed by One-way ANOVA with Bonferroni's post-hoc test and two-sided Student's t-test.. *P < 0.05; **P < 0.01, ***P < 0.001.

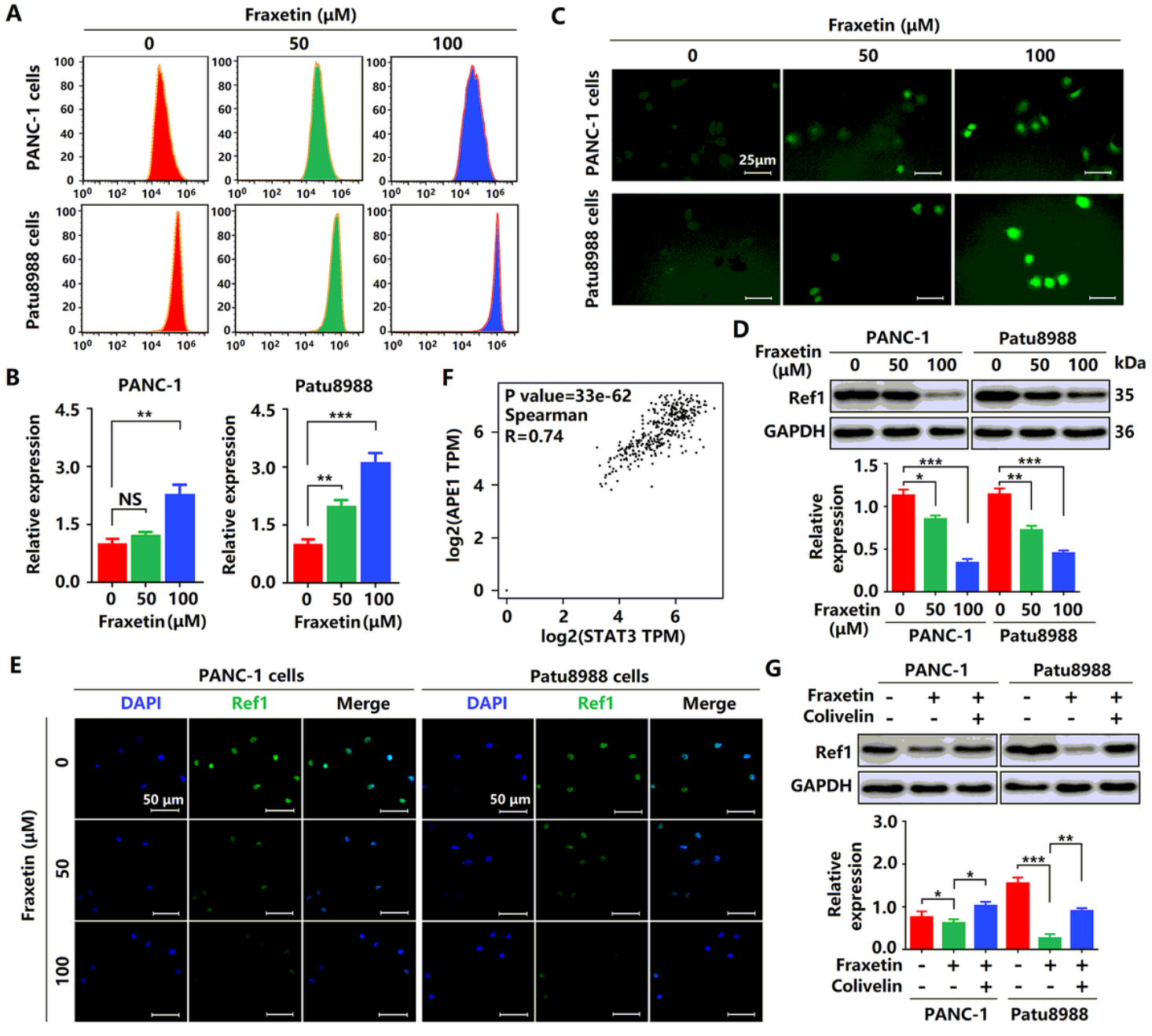

Figure 8

Fraxetin drove ROS-mediated apoptosis by regulating the STAT3-Ref1 axis. (A,B) Flow cytometric analysis showing the levels of ROS in fraxetin-treated PANC-1 and Patu8988 cells. (C) Immunocytochemical staining showing the levels of ROS in fraxetin-treated PANC-1 and Patu8988 cells. Bar = 25 μm. (D) Western blot analysis showing Ref1 expression in fraxetin-treated PANC-1 and Patu8988 cells. (E) Immunocytochemical staining showing Ref1 expression in fraxetin-treated PANC-1 and Patu8988 cells. Bar = 50 μm. (F) The correlation between STAT3 and APE1 (encoding Ref1 protein) in the GEPIA 2 database was evaluated. (G) Western blot analysis showing Ref1 expression in fraxetin-treated PANC-1 and Patu8988 cells with or without colivelin treatment. Data were presented as the mean ± standard deviation, and were analyzed by One-way ANOVA with Bonferroni's post-hoc test and two-sided Student's t-test.. *P < 0.05; **P < 0.01, ***P < 0.001.

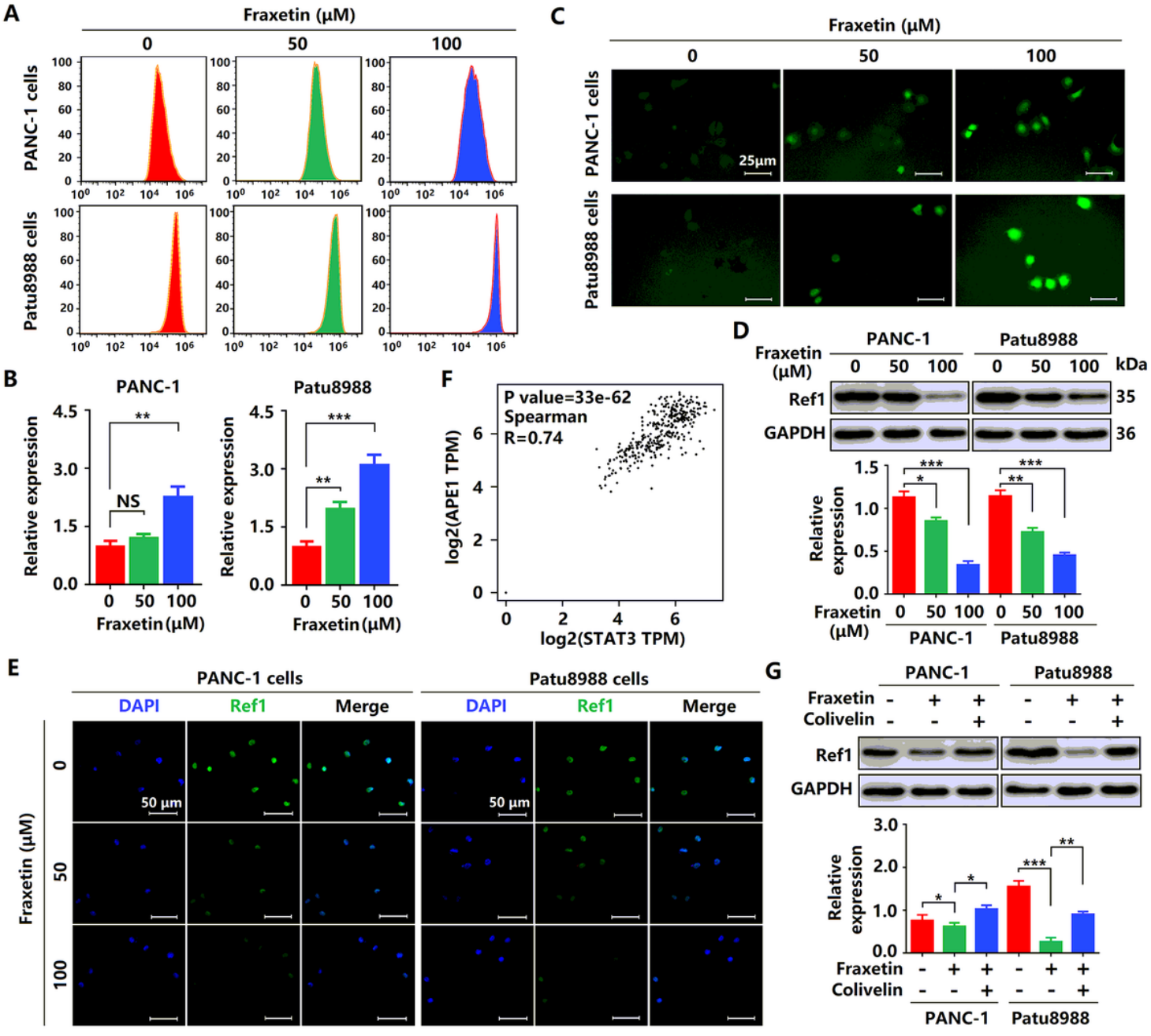

Figure 8

Fraxetin drove ROS-mediated apoptosis by regulating the STAT3-Ref1 axis. (A,B) Flow cytometric analysis showing the levels of ROS in fraxetin-treated PANC-1 and Patu8988 cells. (C) Immunocytochemical staining showing the levels of ROS in fraxetin-treated PANC-1 and Patu8988 cells. Bar = 25 μm. (D) Western blot analysis showing Ref1 expression in fraxetin-treated PANC-1 and Patu8988 cells. (E) Immunocytochemical staining showing Ref1 expression in fraxetin-treated PANC-1 and Patu8988 cells. Bar = 50 μm. (F) The correlation between STAT3 and APE1 (encoding Ref1 protein) in the GEPIA 2 database was evaluated. (G) Western blot analysis showing Ref1 expression in fraxetin-treated PANC-1 and Patu8988 cells with or without colivelin treatment. Data were presented as the mean ± standard deviation, and were analyzed by One-way ANOVA with Bonferroni's post-hoc test and two-sided Student's t-test.. *P < 0.05; **P < 0.01, ***P < 0.001.

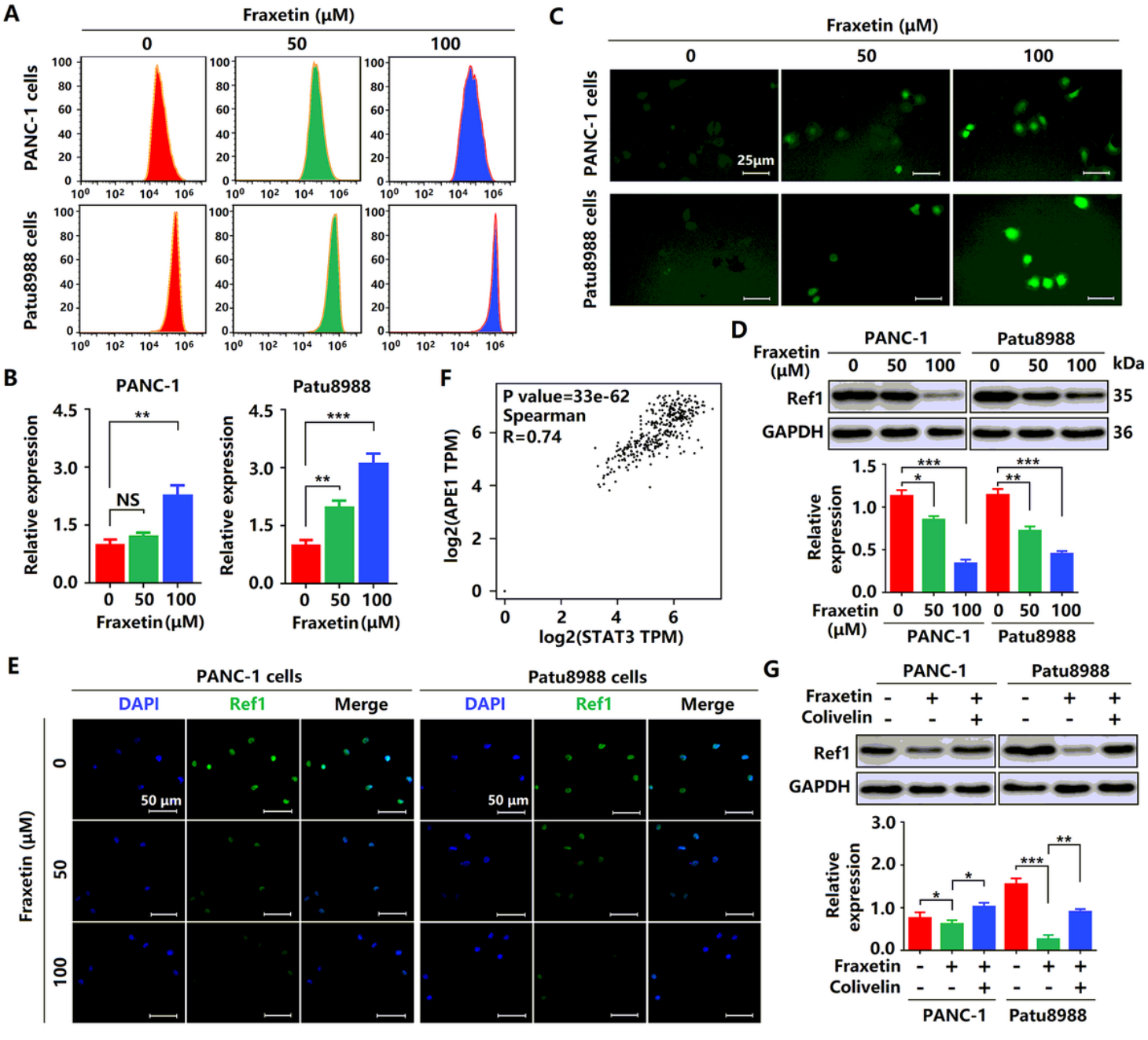

Figure 8

Fraxetin drove ROS-mediated apoptosis by regulating the STAT3-Ref1 axis. (A,B) Flow cytometric analysis showing the levels of ROS in fraxetin-treated PANC-1 and Patu8988 cells. (C) Immunocytochemical staining showing the levels of ROS in fraxetin-treated PANC-1 and Patu8988 cells. Bar = 25 μm. (D) Western blot analysis showing Ref1 expression in fraxetin-treated PANC-1 and Patu8988 cells. (E) Immunocytochemical staining showing Ref1 expression in fraxetin-treated PANC-1 and Patu8988 cells. Bar = 50 μm. (F) The correlation between STAT3 and APE1 (encoding Ref1 protein) in the GEPIA 2 database was evaluated. (G) Western blot analysis showing Ref1 expression in fraxetin-treated PANC-1 and Patu8988 cells with or without colivelin treatment. Data were presented as the mean ± standard deviation, and were analyzed by One-way ANOVA with Bonferroni's post-hoc test and two-sided Student's t-test.. *P < 0.05; **P < 0.01, ***P < 0.001.

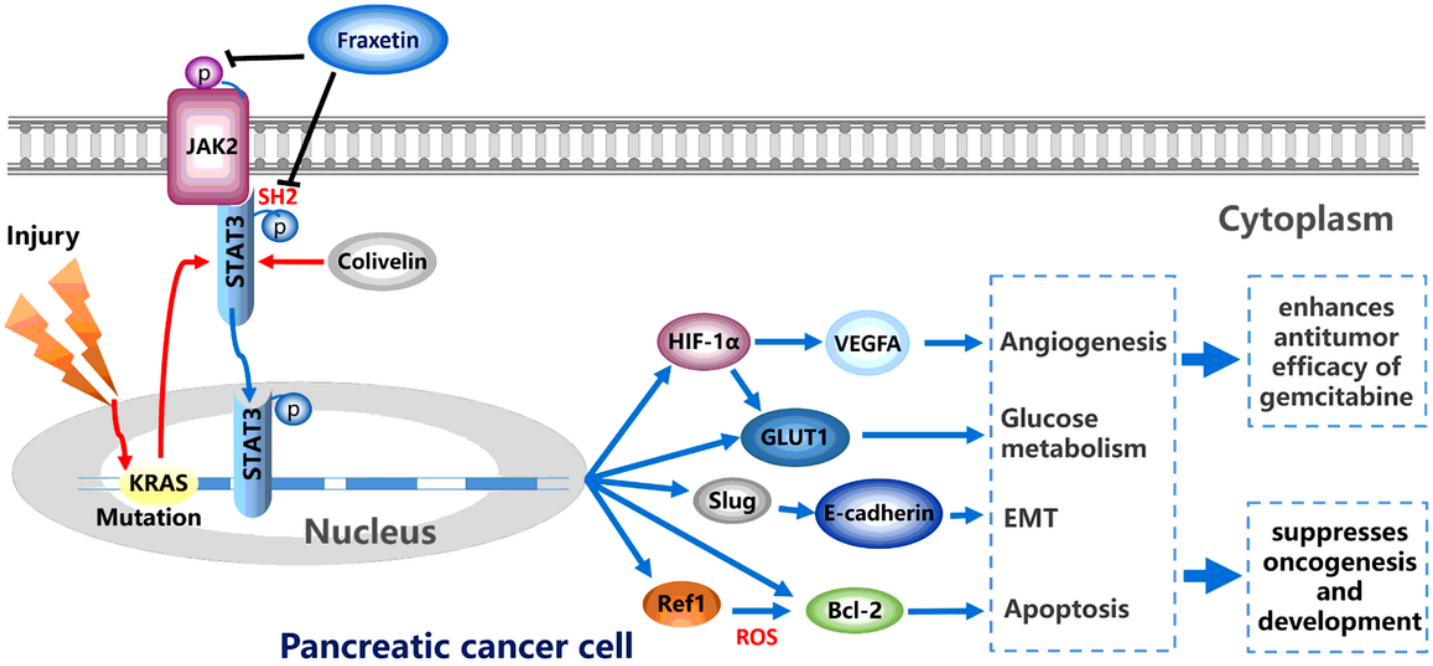

Figure 9

Fraxetin enhances the anti-tumor efficacy of gemcitabine and suppresses oncogenesis and development of PDA via antagonizing STAT3 activation.

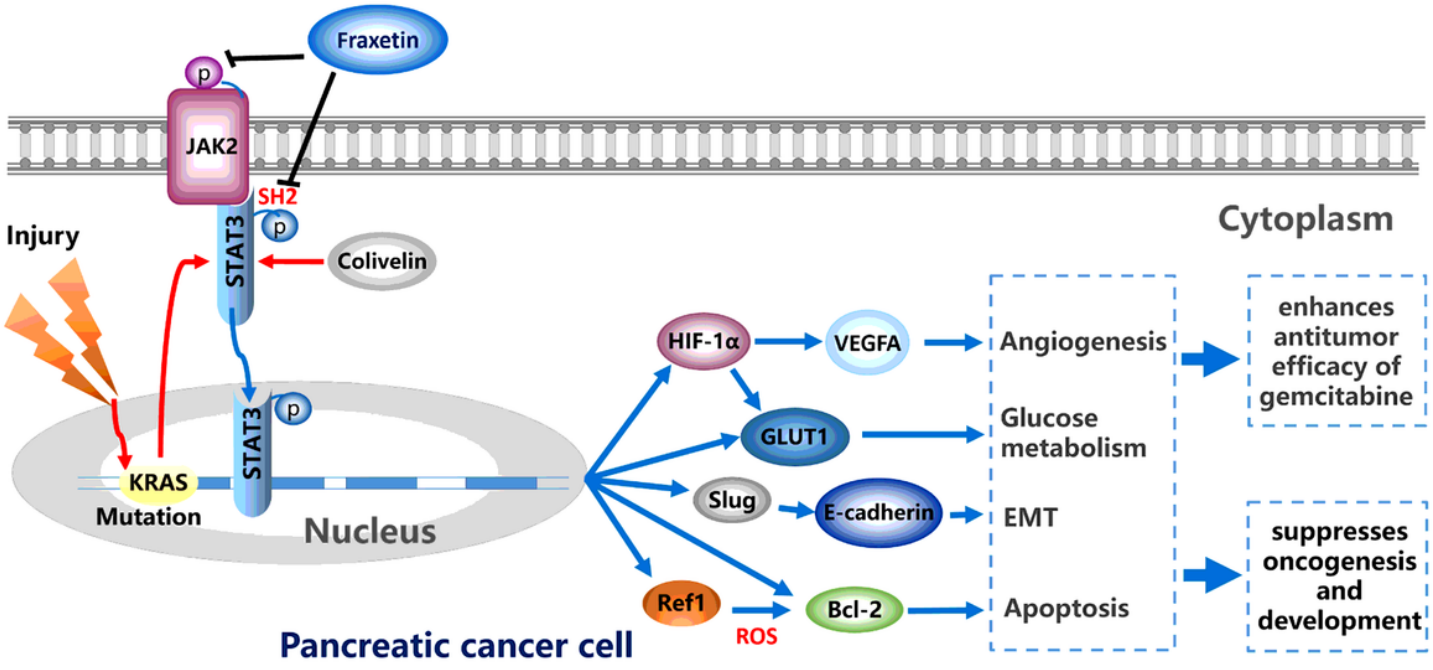

Figure 9

Fraxetin enhances the anti-tumor efficacy of gemcitabine and suppresses oncogenesis and development of PDA via antagonizing STAT3 activation.

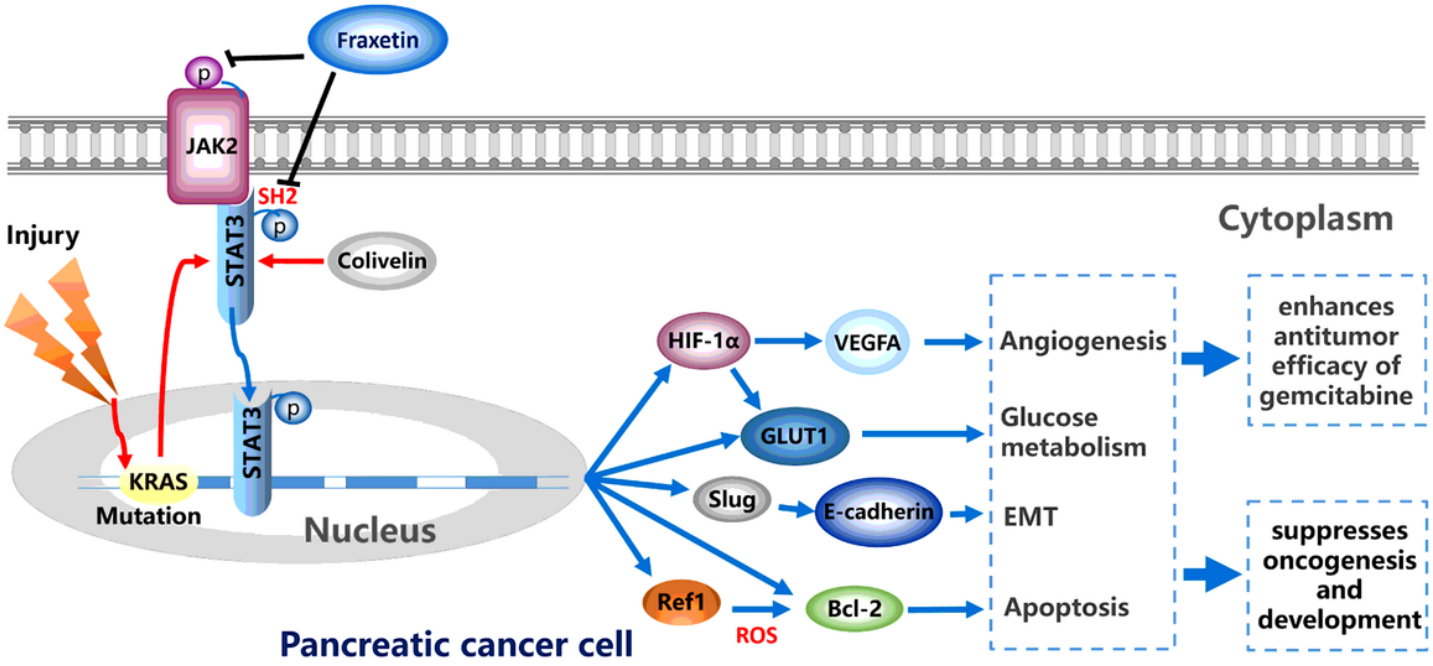

Figure 9

Fraxetin enhances the anti-tumor efficacy of gemcitabine and suppresses oncogenesis and development of PDA via antagonizing STAT3 activation.